Measurement of T_1 relaxation time in lungs

Preclinical and clinical MRI applications to COPD

Daniel Alamidi

Department of Radiation Physics
Institute of Clinical Sciences,
Sahlgrenska Academy at University of Gothenburg,

UNIVERSITY OF GOTHENBURG

Gothenburg 2015

Measurement of T_1 relaxation time in lungs -
Preclinical and clinical MRI applications to COPD

daniel.alamidi@gu.se

ISBN 978-91-628-9525-9 (print)
ISBN 978-91-628-9526-6 (e-pub)
http://hdl.handle.net/2077/39543

Cover illustration: T_1 maps of a mouse and human lung together with corresponding T_1 relaxation plots.

Printed by Ineko AB
Gothenburg, Sweden 2015

“It always seems impossible until it’s done.”

Nelson Mandela

Abstract

Measurement of T_1 relaxation time in lungs
Preclinical and clinical MRI applications to COPD

Daniel Alamidi
Department of Radiation Physics, Institute of Clinical Sciences,
Sahlgrenska Academy at University of Gothenburg,
Göteborg, Sweden, 2015

Monitoring of regional lung function in clinical trials of chronic obstructive pulmonary disease (COPD) requires alternative endpoints beyond global pulmonary function tests (PFTs), which is the most common approach for diagnosing lung function abnormalities in humans. A promising magnetic resonance imaging (MRI) biomarker of lung disease in humans and animals is the T_1 relaxation parameter. Only a limited amount of data on native T_1 behaviour in COPD patients and animal models of COPD are available, especially in relation to other relevant markers such as computed tomography (CT) and PFTs in humans; and bronchoalveolar lavage (BAL) fluid analysis and histology in animals. The smoking history in humans and tobacco smoke (TS) exposure in animals are important factors that need to be investigated in relation to lung T_1 since tobacco smoking is the major cause for development of COPD. Therefore, we have investigated whether lung T_1 can be used as a biomarker of COPD in man, if there is a direct effect of TS on lung T_1 in healthy current smokers, and the repeatability of T_1 measurements acquired at two visits. T_1 was also related to smoking history, CT and PFTs. Subsequently, lung T_1 was investigated in a mouse model of COPD and correlated to BAL, lung mechanics and histology to increase the understanding of how T_1 relates to the pathophysiological aspects of COPD. A preclinical three dimensional (3D) ultra-short echo time (UTE) T_1 mapping protocol was developed to enable the COPD study in mouse. We found from the human studies that: lung T_1 shortens in COPD patients, ageing shortens T_1 and that TS exposure does not affect T_1 in healthy smokers. Additionally, lung T_1 was repeatable and correlated with CT lung density and PFT parameters. Lung T_1 was also shortened in the TS exposed mice, most likely due to early signs of disease. In naive mice, high lung T_1 repeatability over one month was found. In conclusion, lung T_1 mapping is an attractive imaging biomarker of COPD in mouse and man for future longitudinal studies. The potential of MRI-based T_1 mapping to evaluate early COPD has been enhanced by the advances in this thesis.

Keywords: Magnetic Resonance Imaging, biomarker, tobacco smoke, mouse, smoking, lung imaging, Chronic Obstructive Pulmonary Disease, ultrashort echo time (UTE), T1 mapping, longitudinal relaxation time
ISBN: 978-91-628-9525-9 (print)
ISBN: 978-91-628-9526-6 (e-pub)
E-publication: http://hdl.handle.net/2077/39543

Populärvetenskaplig sammanfattning

Inom en snar framtid beräknas kroniskt obstruktiv lungsjukdom (KOL) bli den tredje vanligaste dödorsaken i världen. KOL orsakas av en inflammation i lungorna som oftast beror på rökning. Inflammationen leder till bestående lungskador. Läkemedel kan lindra men inte bota sjukdomen, då KOL är en komplicerad sjukdom som innehåller flera olika komponenter. Dessa komponenter uppenbarar sig inte i alla KOL patienter och varierar över tid. Därför måste behandlingsformen av KOL individanpassas och skräddarsys efter patientens individuella förutsättningar och behov. För att möjliggöra individanpassad medicinering måste biomarkörer användas. En biomarkör speglar en fysiologisk förändring i kroppen som kan bestämmas med magnetkamera.

Bildtagning av lungor med magnetkamera möjliggör biomarkörer för utvärdering av lungsjukdomar. Magnetkameran tar bilder av kroppen med hjälp av magnetfält och radiovågor. Eftersom bildtagningen görs utan joniserande strålning har användningen av magnetkameran ökat vid exempelvis bildtagning av barn och uppföljning av patienter vid kliniska studier.

Relaxationstiden T_1, som kan beräknas från MR-bilder, är en lovande vävnadsspecifik biomarkör för lungsjukdomar. T_1 påverkas av samspelet mellan vatten och andra stora molekyler i kroppen. Hittills har endast ett fåtal studier visat ett samband mellan T_1 och lungsjukdomar. Det saknas dock en förståelse för hur T_1 är relaterat till den bakomliggande patologin för lungsjukdomen. För att öka förståelsen kan med fördel djurmodeller i lungstudier användas där T_1 kan relateras till andra referenser såsom histologi och lungfunktion. Dessutom kan djuren studeras i en kontrollerad miljö jämfört med människor, vilka normalt exponeras för en rad olika faktorer och därmed försvårar utvärderingen av T_1.

Syftet med denna avhandling har varit att utveckla en bildtagningsmetod för utvärdering av KOL i tidigt skede och därmed öka chansen för individanpassad medicinering vid kliniska studier. Vi undersökte om T_1 kan användas som en biomarkör för KOL i både människa och mus. Våra T_1 bestämningar i lungor av KOL patienter, friska rökare och friska försökspersoner visar att T_1 förkortas i KOL patienter, att rökning inte har något direkt samband med T_1, att T_1 förkortas med åldern och att T_1 parametern är repeterbar mellan två besök. I en djurmodell av KOL, dvs. en månads exponering av cigarett rök, kunde vi med det utvecklade robusta tredimensionella T_1 protokollet för mus visa att exponering för cigarettrök medför en förkortning av T_1 i lunga. Denna avhandling har därmed ökat potentialen att använda T_1 mätningar utförda med magnetkamera för utvärdering av KOL i tidigt skede.

Original papers

The thesis is based on the work contained in the following publications, referred to in the text by their Roman numerals:

I. **Alamidi D**, Morgan A, Hubbard Cristinacce P, Nordenmark L, Hockings P, Lagerstrand K.M, Young S, Naish J, Waterton J, Maguire N, Olsson L E., Parker G. *COPD patients have short lung magnetic resonance T_1 relaxation time.* COPD: Journal of Chronic Obstructive Pulmonary Disease, In press, doi: 10.3109/15412555.2015.1048851 (2015).

II. **Alamidi D**, Kindvall S, Hubbard Cristinacce P, McGrath D, Young S, Naish J, Waterton J, Diaz S, Wollmer P, Olsson M, Hockings P, Lagerstrand K.M, Parker G, Olsson L E. *T_1 in lungs of healthy smokers*. Manuscript.

III. **Alamidi D**, Smailagic A, Bidar A, Parker N, Olsson M, Hockings P, Lagerstrand K.M, Olsson L E. *Variable flip angle 3D-UTE T_1 mapping of mouse lung: a repeatability assessment*. Manuscript.

IV. **Alamidi D**, Smailagic A, Bidar A, Parker N, Olsson M, Jacksson S, Swedin L, Hockings P, Lagerstrand K.M, Olsson L E. *Tobacco smoke shortens T_1 in a mouse model of COPD*. Manuscript.

Preliminary reports

The following preliminary reports were given at international meetings:

i. **Alamidi D**, Hubbard P, McGrath D, Pesic J, Zurek M, Gustavsson M, Brunmark C, Naish J, Olsson L E., Parker G. *Similar T_1 changes are found in a translational study in the lungs of human smokers and mice exposed to tobacco smoke*. Annual Meeting of the International Society for Magnetic Resonance in Medicine (ISMRM), Melbourne, Australia, 2012:20:3974.

ii. Zurek M, **Alamidi D**, Johansson E, Risse F, Olsson L E. *Accurate T_1 mapping in rodent lungs using ultrashort echo-time MRI***.** Annual Meeting of the International Society for Magnetic Resonance in Medicine (ISMRM), Melbourne, Australia, 2012:20:3975.

iii. **Alamidi D**, Morgan A, Hubbard Cristinacce P, Nordenmark L, Hockings P, Lagerstrand K.M, Young S, Naish J, Waterton J, Olsson L E., Parker G. *Tobacco smoke exposure reduces lung T_1 in COPD patients*. Annual Meeting of the International Society for Magnetic Resonance in Medicine (ISMRM), Toronto, Canada, 2015:23:977.

iv. **Alamidi D**, Smailagic A, Bidar A, Hockings P, Parker N, Lagerstrand K.M, Olsson M, Olsson L E. *Repeatability of variabile flip angle 3D-UTE T_1 measurements in mouse lung*. Annual Meeting of the European Society for Magnetic Resonance and Biology (ESMRMB), Edinburgh, United Kingdom, 2015:341.

Table of contents

Abbreviations, acronyms and symbols

^{129}Xe	Xenon-129
^{3}He	Helium-3
^{68}Ga	Gallium-68
^{99m}Tc	Technetium-99m
2D	Two-dimensional
3D	Three-dimensional
ADC	Apparent diffusion coefficient
ASL	Arterial spin labeling
B_0	External magnetic field
BAL	Bronchoalveolar lavage
CA	Contrast agent
CO_2	Carbon dioxide
COPD	Chronic obstructive pulmonary disease
CSE	Cigarette smoke extract
CT	Computed tomography
CV	Coefficient of variation, standard deviation as a percentage of the mean
DCE-MRI	Dynamic contrast-enhanced MRI
Diffusion	Process by which molecules spread from areas of high concentration to areas of low concentration
DLCO	Diffusing capacity of the lung for carbon monoxide
FA	Flip angle
FEV_1	Forced expiratory volume in 1 s
FLASH	Fast low angle shot
FOV	Field of view
FVC	Forced vital capacity
GE	Gradient echo
HASTE	Half-fourier single-shot turbo spin echo sequence
HCT	Hematocrit, percentage red blood cells in blood
HU	Hounsfield Units
ICC	Intraclass correlation coefficient
IR	Inversion recovery
M_0	Net longitudinal magnetization at equilibrium
MLI	Mean linear intercept
MRI	Magnetic resonance imaging
M_z	Net longitudinal spin magnetization

O_2	Molecular oxygen
OE-MRI	Oxygen enhanced magnetic resonance imaging
PaO_2	Partial pressure of arterial oxygen in blood
pO_2	Alveolar partial oxygen pressure in lung tissue
PD_{15}	15^{th} percentile density
PET	Positron emission tomography
Perfusion	Flow of blood to reach an organ or tissue
PFT	Pulmonary function test
PY	Number of years in which 20 cigarettes a day was smoked
$r_{1,2}$	Relaxivity
R_1	Longitudinal relaxation rate, $=1/T_1$
R_2	Transversal relaxation rate, $=1/T_2$
RA_{950}	Relative lung area with CT attenuation values below -950
RARE	Rapid acquisition with relaxation enhancement pulse sequence
RF	Radiofrequency
ROI	Region of interest
S_0	Proton density
SD	Standard deviation
SE	Spin echo
SNR	Signal to noise ratio
SI	Signal intensity
SPECT	Single photon emission computed tomography
SPGR	Spoiled gradient echo sequence
T	Tesla
T_1	Time constant for longitudinal relaxation
T_2	Time constant for transversal relaxation due to spin interactions
T_2*	Time constant for transversal relaxation due to a combination of magnetic field inhomogeneities and spin interactions
TE	Echo time of pulse sequence; time between slice excitation and measurement of signal
TI	Inversion time
TR	Repetition time, the amount of time that exists between successive pulse sequences applied to the same slice
TS	Tobacco smoke
UTE	Ultra-short echo time
VA	Alveolar volume
V/Q	Ventilation/perfusion ratio
Ventilation	Exchange of air between the lungs and the atmosphere
VFA	Variable flip angle

1. Introduction

Tobacco smoke (TS) exposure is the main cause for development of chronic obstructive pulmonary disease (COPD), which is projected to rank third in cause of death in a decade (Hanrahan et al. 1996, Marsh et al. 2006). It is a complex and heterogeneous disease, which means that COPD has several components whose dynamic interactions over time are not linear, and that not all of these components are present in all patients at any given time point (Agustí 2013). This awareness underlines the importance of personalising the assessment and treatment of patients with COPD, an emerging field in which imaging biomarkers are likely to play an important role. Additionally, imaging studies performed in both animals and humans are of importance for the understanding of pathophysiological aspects and evaluating new drugs.

Magnetic resonance imaging (MRI) provides attractive biomarkers for the assessment of pulmonary disease in clinical trials as it allows for multiple measurements without the use of ionizing radiation. This is especially important for children, young subjects, pregnant women and placebo cohorts in pharmaceutical trials, where repeated exposure to ionizing radiation needs to be considered carefully given that there may be no clinical benefit of the examination to the subject. Moreover, MRI is minimally invasive, allows regional, structural as well as functional information and is highly translatable between species (Wild et al. 2012, Biederer et al. 2012, Biederer et al. 2012). Lung MRI has been hampered by the low density of the lung and the fast signal decay due to susceptibility differences between tissue and air in lung tissue. Nevertheless, several lung MRI applications have been developed, and interest in MRI of the lungs has recently increased (Wild et al. 2012, Biederer et al. 2012, Biederer et al. 2012).

A promising MRI biomarker of lung disease is the mapping of T_1 relaxation time (subsequently called T_1). T_1 is a physical tissue specific parameter that changes due to interactions of water with macromolecules (Scholz et al. 1989). Moreover, changes in T_1 can reflect regional and global lung function when applied to oxygen-enhanced (OE)-MRI in humans and animals, as T_1 is affected by molecular oxygen (Edelman et al. 1996, Ohno, Hatabu 2007, Ohno et al. 2008, Morgan et al. 2014, Triphan et al. 2014). Thus, T_1 is an attractive potential translational biomarker of lung disease. A few studies

have published data on changes in native T_1 in emphysema (Stadler et al. 2007) and fibrosis (Stadler et al. 2007, Dasenbrook et al. 2013) patients compared to healthy subjects, but no data on lung T_1 behaviour in COPD patients are available, especially in relation to other relevant markers such as smoking history, computed tomography (CT) and pulmonary function tests (PFTs). In animals, only one T_1 mapping study exists that has been applied in a rat model of pulmonary embolism (Togao et al. 2011).

Clearly, there is a gap on the understanding of how T_1 relates to the pathophysiological aspects of lung diseases. There is a need to investigate parameters that affects lung T_1, for example TS exposure which is the main contributing factor to COPD. Like any biomarker, T_1 needs to be properly validated and qualified before investigating response to therapy. In humans, this involves establishment of repeatability and reproducibility. In animal models, this also involves a proper characterization of T_1 against invasive markers like bronchoalveolar lavage (BAL) fluid and histology.

1.1 Aims

The aims of this thesis are:

1. To investigate if lung T_1 can be used as a biomarker of COPD in mouse and man (**Paper I&IV**).
2. To investigate whether there is a direct effect of tobacco smoke exposure on lung T_1 (**Paper II&IV**).
3. To develop and evaluate a preclinical three-dimensional (3D) protocol for T_1 measurements in the lungs with ultra-short echo time (UTE) with a view to test potential new medicines for COPD (**Paper III**).

Ultimately the purpose is to have a sensitive, non-invasive, radiation-free and translational imaging method to evaluate the early phase of COPD, thus enhancing the chance of pharmaceutical interventions and facilitating patient stratification in clinical trials.

2. Background

2.1 The lung

The main function of the lung is to transport oxygen (O_2) into the body and release carbon oxide (CO_2). When air enters the lungs, it travels via the oral cavities down to the trachea that divides into two main bronchi (Figure 1). Here, the bronchi diverge into two daughter branches to a system of small bronchi and bronchioles until the alveoli are reached. The alveoli are closely packed air sacs, like individual grapes within a bunch. The lung can be regarded as a network of these small 500 million bunches. Each individual alveolus is tightly wrapped in blood vessels, allowing gases in the alveoli to easily diffuse into and out of the blood (Faller et al. 2004).

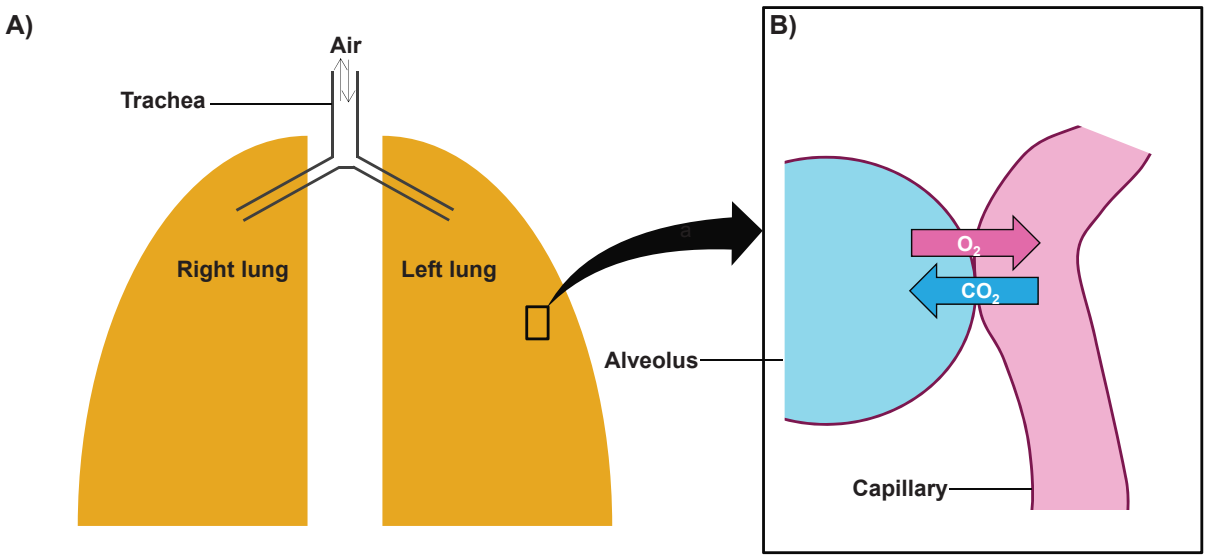

Figure 1. A) Schematic illustration of the lungs. B) Enlarged Lung tissue of the gas exchange showing one alveoli with a corresponding capillary. The airways are made up by a branching network of thin tubes which ends up in a bunch of alveoli. These alveoli are little grape-like air sacks surrounded by a capillary network. The exchange of gases in the lung transforms deoxygenated venous blood that is rich in CO2 into oxygenated arterial blood with low CO2 content.

The alveolar walls are covered with pulmonary surfactant, a lipoprotein. The surfactant prevents alveolar collapse and increase pulmonary compliance, i.e. the lung's ability to stretch and expand. The extracellular matrix consists of several different cell types that surround and support the airways, alveolar cells and the vascular system. Collagen is the most abundant macromolecule that acts on the alveolar fiber network with major contribution in lung mechanics.

2.1.1 The breathing mechanism

Lung function is driven by the diaphragm; the thin, dome-shaped muscle at the base of the thoracic cavity. During inspiration, the volume of the thoracic cavity increases and air is drawn into the lung. The volume increase causes the internal pressure of the chest to become lower than atmospheric pressure, resulting in a flow of air into the airways. The driving forces for gas exchange between the lung and the environment are the pressure differences.

The process of *internal respiration* comprises the exchange of O_2 and CO_2 between blood and cells in different tissues. In contrast, *external respiration* is the process by which outer air is drawn into the body in order to supply lungs with O_2, and "used" air is expelled from the lungs in order to remove the CO_2 from the body.

The oxygen transport can be divided into three steps: (1) *Ventilation*, or breathing, involves the physical movement of air in and out of the lungs; (2) *Gas diffusion,* exchange of gases between the alveoli and the pulmonary capillaries; (3) *Perfusion*, circulation of blood between the lungs and organs (Faller et al. 2004).

2.1.2 Comparison of mouse and human lung

Our current understanding of the lung function and lung disease mechanisms comes to a great extent from studies applied in animals. Mice are widely employed in lung research because of a well-understood immunologic system, a short reproductive cycle, a well-characterized genome, the application of transgenic technology and economic factors. However, the structure of the mouse lung is significantly different than the human lung. The total lung capacity (TLC) of the mouse is about 1 ml compared to 6,000

ml of a human. The human lung has three right lobes and two left lobes and the mouse lung has four right lobes and a single left lobe (Irvin, Bates 2003).

Furthermore, rodents have larger lung density than humans and the alveoli of the mouse lung (40 μm mean linear intercept (MLI)) are smaller than those of human (MLI 200 μm) (Lum, Mitzner 1987, Olsson et al. 2007a, Lederlin, Crémillieux 2014). The diffusion distance of the blood-gas barrier thickness, in the mouse (0.32 μm) is almost half as thick as in the human (0.62 μm), which might have important consequences for both gas exchange and lung mechanics. Mouse lungs have fewer respiratory bronchioles and airway generations (13-17 generations) than human lungs (17-21 generations) (Irvin, Bates 2003).

Finally, mice have high respiratory rates ~160 breaths/min, and high cardiac rates, ~600 beats/min, compared to humans with 12-70 breaths/min and 70 beats/min (Irvin, Bates 2003).

2.1.3 COPD and other lung diseases

In case of lung disease, many of the properties and mechanics governing lung function are impaired. Emphysema is a lung disease with low lung density arising from the destruction of alveolar walls (Thurlbeck, Muller 1994). The abnormal permanent enlargement of airspaces leads to a loss of lung elasticity making it difficult to exhale as the lung collapses. Pulmonary emphysema is classified into three major types based on the disease distribution within secondary pulmonary lobules: centrilobular, paraseptal and panlobular emphysema. Pulmonary fibrosis occurs when lung tissue becomes stiff and scarred leading to serious breathing problems (Katzenstein, Myers 1998). In case of an inflammation of the lung tissue, for example, plasma leakage into the alveoli increases the diffusion distance and impairs alveolar gas exchange. Additionally, the accumulation of inflammatory cells leads to thickening of the bronchial walls causing reduced O_2 supply into the blood.

One of the most significant lung diseases is COPD. It is a complex heterogeneous inflammatory airway disease characterized by a slowly progressive and irreversible airflow obstruction, loss of lung tissue leading to emphysema, and fibrosis (Stockley, Mannino & Barnes 2009). Bronchiectasis, enlargement of airways as a result of infection, bronchiolitis

and inflammation of the smallest airways are further general pulmonary changes in connection to COPD.

Animal models of COPD have been used effectively and are of critical importance to study the pathogenesis of this disease and potential therapeutic interventions (Shapiro 2000). Murine models of TS that induce lung inflammation and lung damage have become the preferred preclinical system for investigating pathologies associated with COPD (Stevenson, Birrell 2011), as tobacco smoking is the major risk factor for COPD, and induces both emphysema and fibrosis (Mannino et al. 2006).

In respiratory disorders such as COPD, alterations in the ventilation and/or perfusion continue to progress and gas diffusion between the alveoli and the capillaries is impaired. These abnormalities lead to a reduction in the outflow of air during expiration that can be assessed by PFT measurements (Devereux 2006).

2.1.4 Lung function measurements for COPD

In humans, characterization of COPD relies on spirometry based PFT measurements, such as forced expiratory volume in 1 s (FEV_1), forced vital capacity (FVC) and the diffusing capacity for carbon monoxide in the lung (DLCO) (Pauwels, Rabe 2004). The DLCO is often adjusted for the alveolar volume (VA). Spirometric lung function tests are inexpensive, relatively easy to perform and are therefore commonly used in the clinic as well as in large cohort clinical studies. In combination with spirometric measures, arterial blood gas analysis measurements such as partial pressure of oxygen (PaO_2) are used to estimate oxygen supply and determine gas exchange across the alveolar-capillary membrane. However, these methods only measure global lung function and can only diagnose impaired lung function when the disorders of the lung have reached more advanced stages (Bergin et al. 1986, Swanney et al. 2008). Impaired lung function originates locally, and often differ from one lung region to another. In mice, the available standard method for lung function measurements is forced invasive ventilator measurements with the FlexiVent system. However, FlexiVent only results in one-time point measurements because tracheostomy is mandatory and this is a terminal procedure.

2.2 Lung imaging methods not based on MRI

The inconsistency between spirometric lung function measurements and disease symptoms, as well as the nonspecific differentiation of lung disorders, has led to increasing interest in image based methods for the diagnosis and classification of COPD (Stockley, Mannino & Barnes 2009, Roy et al. 2009, Costa et al. 2009, Jones, Agusti 2006). Depending on the application, there are a number of lung imaging techniques available that in one way or another depict detailed information on a regional level. There are two main areas of lung imaging research: structural imaging that aims to depict the lung with high resolution detailed 3D imaging, and functional imaging that aims to demonstrate, for example, regional perfusion and ventilation of the lung. This subchapter provides an overview of existing non-MRI lung imaging methods and finally summarizes the main characteristics of the modalities in Table 1 (van Echteld, Beckmann 2011, van der Have et al. 2009, Yamamoto et al. 2011, Schaefer-Prokop et al. 2008).

2.2.1 Chest X-ray

Traditionally, standard chest x-ray is used for lung structure imaging to detect lung abnormalities such as pneumonia, pulmonary nodules etc but may also reveal changes of emphysema. Such images are inexpensive, easily obtained and involve minimal radiation exposure. However, a chest x-ray does not provide 3D or functional information.

2.2.2 Nuclear medicine based techniques

The workhorse for imaging of lung function in the clinic has been planar scintigraphy and 3D imaging with single photon emission computed tomography (SPECT) using radioactive labeled tracers (Jögi et al. 2011). Ventilation measurements are performed by inhalation of gaseous radionuclide, such as technetium-99m (^{99m}Tc), in an aerosol form, and perfusion is measured by intravenous injection of ^{99m}Tc macroaggregated albumin. The ventilation/perfusion (V/Q) examination is primarily used to diagnose pulmonary embolism, but also to detect and stage the degree of airway obstruction. Another nuclear medicine technique, positron emission tomography (PET), can also be used to study V/Q ratio, by substituting ^{99m}Tc with Gallium-68 (^{68}Ga), a positron-emitting radionuclide. PET/CT ventilation imaging is performed with ^{68}Ga-carbon nanoparticles and perfusion can be performed with ^{68}Ga macroaggregated albumin (Hofman et al. 2011). Moreover, drug deposition in the lung can be assessed with inhaled radiolabelled aerosols. Nuclear imaging techniques provide functional information with high sensitivity, however, besides the exposure to ionizing

radiation and time consuming examinations, nuclear imaging techniques have poor spatial resolution (Bauman and Eichinger 2012) (Table 1).

2.2.3 Computed tomography

The standard imaging modality for visualization and quantification of regional changes in lungs of subjects with COPD, particularly emphysema is CT (Karimi et al. 2014, Ashraf et al. 2011, Wille et al. 2014, Coxson et al. 2013). CT is more sensitive than chest x-ray and PFTs (Takahashi et al. 2008) in detecting and characterizing diseases. A CT scanner can, in principle, be used as a densitometer as the brightness of each voxel is a product of the density of the tissue it encompasses. The density is expressed in Hounsfield Units (HU) and normally ranges from -1000 HU in air, through 0 HU in water, to +1000 HU in bone. This information can be used to generate a histogram of the distribution of tissue densities in the lung, where each point is defined by the HU value of that voxel. The extent of emphysema is objectively identified at total lung capacity by two common methods where meaningful points on the CT lung histogram exist; the 15^{th} percentile density (PD_{15}) and the relative lung area with CT attenuation values below -950 HU (RA_{950}). PD_{15} is a percentile point that delineates the lowest 15% of the histogram from the denser 85%. RA_{950} is a fixed HU threshold below 950, to identify the low attenuation regions of emphysema.

Lung CT can define COPD into emphysema-predominant and airway-predominant forms (Lynch 2008, Nakano et al. 2000) by measurements of airway wall thickness and the extent of emphysema in the same patient at the same time. Functional parameters such as perfusion and ventilation can be assessed by dynamic and dual-energy CT after the administration of contrast medium. For perfusion, an iodinated contrast agent is injected and for ventilation, gaseous nonradioactive xenon is used. The main applications have been to demonstrate ventilation changes, pulmonary embolism and hypertension or characterization of lung tumors (Mirsadraee, van Beek 2015).

Micro-CT provides non-invasive structural evaluation of small animals. Repetitive measurements of micro-CT, however, may expose the animal to ionizing radiation doses sufficiently high to induce biological side effects. Thereby the experimental conditions and possible outcomes might be affected (Boone, Velazquez & Cherry 2004). Particularly at high spatial resolution imaging, the smaller voxel size requires significantly higher radiation dose to produce images comparable to clinical CT.

Although CT is a powerful tool for pulmonary imaging and a workhorse in numerous COPD studies, it has several limitations. Firstly, exposure to ionizing radiation limits the extensive use of CT in longitudinal assessments. Secondly, functional imaging with CT is complicated, since it is associated with high costs, adverse effects and requires specialized expertise and equipment. Thirdly, current CT resolution is high, but not sufficient to completely resolve the small airways < 2 mm that are the main site of airflow obstruction in COPD. Therefore, imaging techniques that allows follow-up examinations without cumulating radiation dose and comprehensive functional imaging are desirable, such as MRI. Moreover, CT imaging only reflects one contrast mechanism; electron density, which provides far less soft tissue contrast than MRI.

Table 1. Comparison of imaging modalities for lung research.

Technique	Spatial resolution		Application	Main Characteristics
	Small animals	Humans		
X-ray	100 µm	100 µm	Structural	Planar information
Scintigraphy	1 mm	~20 mm	Functional	Planar information
SPECT	<1 mm	~10 mm	Functional	Ionizing radiation
PET	1-2 mm	~4 mm	Metabolic, functional, molecular	Ionizing radiation; high sensitivity cyclotron needed
CT	50-100 µm	200-300 µm	Structural, functional	Ionizing radiation; poor soft tissue contrast
MRI	80-140 µm	~1 mm	Structural, functional, molecular	High spatial resolution and soft tissue contrast; low sensitivity

2.3 MRI of the lung

The recent technological developments of MRI have enabled many scientific and clinical applications for lung imaging (Wild et al. 2012). MRI scanners use powerful external magnetic fields and radio waves to create images of the body without exposure to ionizing radiation. The central technique for MRI is based on the resonant frequency signal of protons in tissues and liquids. Lung MRI enables improved soft tissue contrast with 3D coverage of morphologic and functional information due to recent improvements in gradient systems and reconstruction methods (Biederer 2005, Kruger et al. 2015). In this subsection, an overview of most common lung MRI methods is provided, starting with the challenges of conducting pulmonary MRI in both humans and animals. The majority of this section is written for human applications.

2.3.1 Challenges with lung MRI

Lung MRI is facing many difficulties because of the morphology, physiology and composition of the lung in comparison to other tissues such as liver or brain. Due to the air within the lung, the lung has inherently low average proton density (S_0) generating weak signal, resulting in relatively low signal to noise ratio (SNR). Water density in the lung varies from 10 to 25% depending on inflation level (Theilmann et al. 2009), compared with 80 to 90% for most body tissues. The major obstacle for straightforward MR imaging of the lungs is the magnetic susceptibility difference caused by the multiple air-tissue interfaces within the alveoli in the lung. The heterogeneous microstructure of lung parenchyma creates local magnetic gradients that rapidly dephase the already low MR signal. The rate of signal decay, T_2*, varies in human lung depending on lung inflation from about 1 ms at total lung capacity to 2 ms at residual volume in clinical applications at 1.5 T.

Furthermore, imaging of thoracic organs presents additional challenges due to the continuous physiological motion induced by heart pulsation and respiration that can be reduced with breath-holding or gating methods. However, breath-holds can be very demanding for patients in poor respiratory conditions and a drawback of gating techniques is a prolonged acquisition time.

Additional to these technical challenges, the MR signal from the lung is sensitive to several physiological parameters, such as the state of inflation and the oxygenation of the blood. Therefore, the signal generation can be quite complex and it can be hard to identify the relationship between changes

in the signal of the lung parenchyma and underlying physiological properties of the lung.

2.3.1.1 Differences and challenges in lung MRI for humans and small animals

Conventional high field clinical MRI scanners have magnetic field (B_0) strengths between 1.5 and 3 tesla (T). In contrast, small animal MRI scanners operate at even higher B_0, i.e. 4.7 T to 9.4 T. The SNR is roughly proportional to the B_0. Thus, the higher B_0 enable the SNR needed to achieve the necessary spatial resolution for the smaller animals. However, the higher B_0 shortens the T_2* of the lung, 0.5 ms for free-breathing mice at 4.7 T (Olsson et al. 2007b) compared to about 2 ms (Yu, Xue & Song 2011) for free-breathing human lungs at 1.5 T. Additionally, the gradients of small animal systems are typically 10-50 more powerful than those of a clinical system (20 mT/m) to achieve the higher spatial resolution needed compared to humans.

Imaging of the thorax can be more troublesome in rodents than in humans, because of the higher cardiac and respiratory rates. Gating techniques can be used to avoid artifacts by triggering the acquisition to the breathing cycle or the electrocardiogram, and/or mechanical ventilation. However, in pharmacological studies of airway disease, it is important to keep experiment conditions as straightforward as possible so that repeated measurements interfere minimally with the physiology. Gating techniques can send a trigger signal to the scanner to synchronize image acquisition with the specific phase during the breathing cycle, but will increase the complexity of the MR protocol and the acquisition time. A mechanical ventilator can also be used to control the breathing cycle and thereby guide the acquisition. However, it relies on intubation, by inserting a tube into the trachea which requires skilled assessment and performance, or tracheostomy which prevents follow-up studies, as only one imaging session per animal can be performed. More importantly, mechanical ventilation interferes with the natural physiological breathing, it might cause lung injury complications (van Echteld, Beckmann 2011) and makes the animal experiment more complex. Alternatively, motion artifacts in lungs can be reduced with signal averaging without any gating (Blé et al. 2008).

In summary, MRI of small animals provides non-invasive means to assess tissue structure and function in a 3D fashion without the exposure to ionizing radiation. It allows longitudinal monitoring of treatment which serves to minimize the number of animals required for a specific study and thereby increasing the statistical power of experiments. Each animal can also serve as

its own control and thereby reduce the biological variability. Consequently, MRI is an ideal candidate for a broad range of imaging tasks in biomedical preclinical respiratory research.

2.3.2 Lung MRI pulse sequences

A variety of different pulse sequence and acquisition techniques have been developed to address the lung MRI challenges for both humans and animals (section 2.3.1). One of the simplest and most common lung MRI sequences is a conventional gradient echo (GE) with short echo time (TE) in the ms range. The short TE for a GE is essential to maintain image quality of the lungs (Johnson et al. 2013). Nevertheless, this property can be used as an asset, since pathologies with higher S_0 in the lung will stand out against the black background of healthy lung parenchyma. The T_2* in the lung is still long enough in humans to obtain valuable signal from GE acquisitions with short TEs, for instance to measure water density in the lung (Theilmann et al. 2009). Moreover, the spoiled GE sequence (SPGR) has multiple applications in lung MRI such as anatomical imaging and dynamic acquisitions that enable motion assessments of the lung wall, tumours and the diaphragm (Wild et al. 2012).

Since the T_2 is much longer than T_2* in the lung in humans, around 40 ms (Buzan et al. 2015), spin echo (SE) techniques makes it possible to obtain useful SNR in lung using fast SE sequences such as HASTE (half-Fourier acquisition single-shot turbo spin-echo) (**Paper I**).

UTE imaging with radial readouts have proven to be promising for lung imaging of human and animals as it provides TEs in the μs range to increase SNR and maintain image quality. The radial k-space sampling from the center of k-space makes UTE sequences less sensitive to motion, as compared to Cartesian acquisition. Acquisitions with UTE can be formed without the need of gating due to the effective reduction of motion artifacts of the radial sampling (Lederlin, Crémillieux 2014, Takahashi et al. 2010) (**Paper III&IV**). Volumetric acquisitions of the human lungs with 3D UTE allows high spatial resolution, ~1 mm, with a S_0 contrast approaching that of CT (Kruger et al. 2015, Ohno et al. 2015).

2.3.3 Lung MRI perfusion

Perfusion is the amount of arterial blood delivered to a tissue in a certain time period (Kauczor, Altes 2009). Pulmonary perfusion is altered in various diseases of the lung such as pulmonary hypertension and fibrosis. The most common perfusion MRI method in the clinic, dynamic contrast-enhanced MRI (DCE-MRI), is based on the tracking of the T_1 weighted signal during the first passage of a contrast agent (CA), such as paramagnetic gadolinium chelates, in the lung (Togao et al. 2011). The tracking of the signal enhancement is performed using continuous 3D T_1-weighted GE imaging with short repetition time (TR) and TE. DCE-MRI has improved SNR over non-contrast imaging and is relatively easy to use. However, it cannot be repeated arbitrarily and there is a limit in the total amount of CA that can be introduced into the patient.

Another perfusion imaging technique, arterial spin labeling (ASL) utilizes magnetically tagged water protons in blood as a contrast bolus to measure blood perfusion in the lung. The proton spins in the blood are tagged with inverted radiofrequency (RF) pulses to perturbate the magnetization. The evolution of the spins in the inflowing blood is then measured in the lung parenchyma. ASL is derived from the subtraction of two acquisitions, a control and a tagged acquisition with different schemes of magnetization inversion. In the clinic this non-invasive technique is difficult to implement due to respiratory motion, signal change induced by blood flow in larger vessels and the prolonged examination times (Walker et al. 2015).

Recently, the Fourier decomposition method has been proposed for non-invasive lung function MRI. FD provides both ventilation and perfusion images of the lungs with neither CA nor respiratory gating. Free breathing imaging is performed with a two-dimensional (2D) balanced steady-state free precession (bSSFP) sequence to derive time-resolved data stacks. Perfusion and ventilation images are produced by Fourier analysis and post processing of the data. However, the quantitative signal analysis of this technique needs further investigation (Bauman et al. 2009).

2.3.4 Lung MRI ventilation

Ventilation by MRI is mainly achieved by inhalation of oxygen or hyperpolarized gases. Dissolved molecular oxygen causes a T_1-shortening of the blood and provides means to study regional and global lung function influenced by ventilation, perfusion and alveoli diffusion (Edelman et al.

1996). 3D radial UTE shows promise as a method for OE-MRI in both small animals and humans (Kruger et al. 2015, Ohno et al. 2015). This method can produce 3D maps of oxygen enhancement, a measure of the lung's oxygen exchange. This can be applied to patients with lung abnormalities and result in regional information on perfusion-ventilation mismatch. The technique is remained in a research setting and requires standardized image post-processing tools before going into clinical practice.

Hyperpolarized gas MRI using helium-3 (^{3}He) has been developed to improve imaging of lung ventilation. Pulmonary imaging with hyperpolarized ^{3}He has excellent SNR properties and has been applied in studies of different pulmonary diseases including emphysema, cystic fibrosis and COPD (Mirsadraee, van Beek 2015). The main limitations with ^{3}He MRI are its limited gas supply, the required sophisticated equipment and the expensive price of helium gas.

Due to a shortage of ^{3}He interest has been directed to xenon-129 (^{129}Xe) gas imaging during the last decade. In addition to be used for ventilation the gas is highly soluble and can diffuse into blood which offers new insights of functional parameters such as gas exchange and uptake, compared to ^{3}He MRI. Even though both hyperpolarized ^{3}He and ^{129}Xe lung imaging has shown a great potential in both preclinical and clinical applications, ^{129}Xe and ^{3}He MRI have remained limited to advanced research centers since dedicated equipment and expertise is required to produce these hyperpolarized gases (Mirsadraee, van Beek 2015).

2.4 The MR signal and lung relaxation times

One of the most fascinating characteristics of MRI is the many sources of image contrast which affects the MR signal and the numerous ways in which their respective influences may be controlled by the pulse sequences. The contrast in MR images evolves from for example: perfusion, diffusion, S_0 and the considerable differences of tissue relaxation times. The relaxation times of protons in biological systems are known to be affected of a variety of factors, such as macromolecule content. Therefore, understanding their independent effects is critical for proper interpretation of the specific quantification. A summary of factors affecting relaxation times are presented in Table 3 in section 2.4.3.

2.4.1 T_1 relaxation time

There are two energy states the hydrogen nucleus can occupy in the presence of an external B_0; the lower energy state where the magnetic dipole moment are aligned to B_0, or the higher energy state where the magnetic dipole moment are aligned opposite to B_0. At thermal equilibrium, a slight surplus of dipoles are observed in the lower energy state along B_0 creating a net magnetization. After a 90° RF pulse, the system with the net magnetization will be perturbed from its equilibrium position to the high energy state. To release energy and return to the lower energy state, the protons interact with the protons attached to the surrounding molecules, the lattice, which can absorb the energy. In order to enable this energy transfer, the magnetic dipole moments of the neighbouring protons or other nuclei or molecules has to fluctuate at the *Larmor frequency* and thereby satisfy the resonance condition. Due to the fluctuating fields the spins can change from high to low energy states through interaction with the lattice, and contribute to a relaxation in magnetization. T_1 relaxation time (also known as thermal, longitudinal or spin-lattice relaxation) is defined as the time it takes for M_z to recover to a value about 63 % of M_0 after a 90˚ RF excitation of the longitudinal magnetization.

Accordingly, longitudinal relaxation can occur only when a proton encounters another magnetic field fluctuating near the Larmor frequency and the frequency and intensity of these fluctuations differ in different types of tissue. T_1 will therefore be affected by the mobility of molecules, particularly water molecules, and the binding of water molecules, for example to macromolecules. T_1 in tissues varies from several seconds in water fluids to

less than 300 ms in fat. Table 2 summarizes T_1 values for different tissues collected from in house measurements and the literature (Triphan et al. 2015, Gold et al. 2004, Barth and Moser 1997, Silvennoinen, Kettunen & Kauppinen 2003b, Bottomley et al. 1984, Laurent, Bonny & Renou 2000, Deoni, Peters & Rutt 2004).

Table 2. T_1 relaxation times (ms) of tissues and water at 1.5 T in human and 4.7 T in mouse.

Tissue	T_1 (ms) at 1.5 T Human	T_1 (ms) at 4.7 T Mouse
Lung, short TE*	1060[a]	1260[‡]
Lung, long TE**	1390[a]	1560[‡]
Muscle	1130[b]	1430[‡]
Blood	1430[c]	1700[d]
Fat	260[e]	350[f]
Water	3160[g]	3560[‡]

*TE at 1.5T = 70 μs, 4.7T = 8 μs with VFA 3D-UTE
**TE at 1.5T = 2.3 ms, 4.7T = 4 ms with 2D IR-RARE
‡In house experiments
[a]Triphan *et al*., [b]Gold *et al*., [c]Barth and Moser, [d]Silvennoinen *et al*.
[e]Bottemley *et al*., [f]Laurent *et al*., [g]Deoni *et al*.

2.4.2 Factors affecting the MR signal

The MR signal can be modulated to allow quantification of tissue specific parameters such as S_0 and T_1. The signal intensity (SI) from the lung arises from a complex mixture of several components that can be summarized into three main compartments: tissue *water* in the lung parenchyma, water bound to *macromolecules* (collagen) and circulating *blood* (Figure 2). The signal generated within each single image voxel in lung is an amalgam of the various kinds of tissue such as blood, vessels and alveolar cells in the voxel (Nakagawa et al. 2001, Chen et al. 1998).

The S_0 is related to the inflation of the lung and an inverse linear relationship between *lung volume* and SI has been found by Bankier *et al*. (Bankier et al. 2004). The signal behaviour of the lung at different respiratory phases has been studied by Mai et al. who found larger SNR at end expiration (Mai et al. 2000). A 100% increase of lung SNR between end-expiratory and end-inspiratory breath-holding was found.

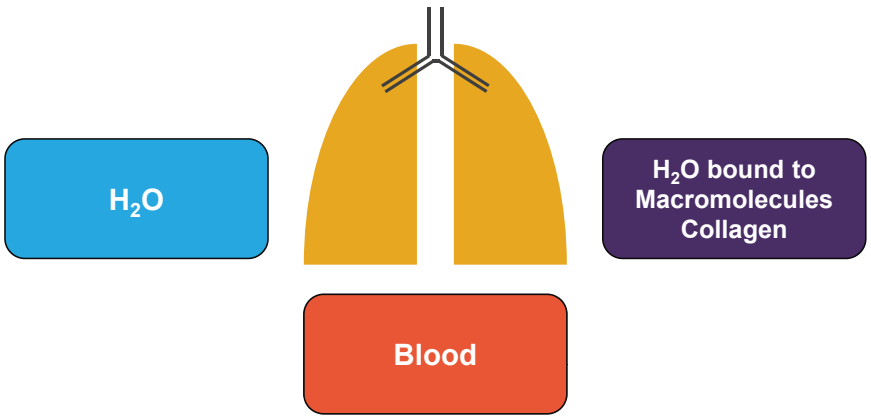

Figure 2. The MR signal in lung arises from three main compartments; water in tissue and interstitial spaces, water bound to macromolecules (collagen) and perfused blood.

2.4.3 Factors affecting the T_1 and T_2* relaxation times

The lung signal, which arises from the three compartments mentioned above, can be separated into blood and water protons. Triphan *et al*. found that the detectable signal from protons in lung is highly dependent on the *TE* (Triphan et al. 2015). Both lung compartments are reflected at very short TEs. As TE increases, the blood protons will dominate as signal from the water protons in the lung parenchyma dephases. Since blood has a longer T_1 than lung parenchyma, lung T_1 will increase as TE increases.

Monitoring the *temperature* during scanning is important especially in a preclinical setting. Kveder *et al*. (Kveder et al. 1988) found that T_1 increases with increasing temperature on isolated rat lungs. Moreover, Kveder *et al*. showed that T_1 in lung tissue increases at higher *magnetic field* (B_0).

Stadler *et al*. has found that lung T_1 is shorter in full *inspiration* than full expiration (Stadler et al. 2005). The observed finding with shortened T_1 for increased lung *volume* most likely reflects elimination of long T_1 compartments such as blood and water as the lung expands.

2.4.3.1 Blood

Normal human lungs in the body contain around 1000 g of tissue and blood of which half is tissue and half is blood (Armstrong et al. 1982). Accordingly, around 500 ml or 10% of the total circulating blood volume is in the pulmonary circulation which will have a significant effect on the local magnetic environment and the pulmonary MR signal. Hence, a gravity effect of circulating blood in the lung is present, resulting in an uneven distribution of blood (Hopkins et al. 2007). This uneven distribution of blood might have implications on regional lung T_1 values and therefore increase the variation of T_1 in the lung. The gravity dependent lung regions will have longer T_1 as blood has longer T_1 than lung tissue.

Relaxivity ($r_{1,2}$ in units of $M^{-1}s^{-1}$) is the ability of magnetic compounds to increase the *relaxation rate* ($R_{1,2}=1/T_{1,2}$ in units of s^{-1}) of the surrounding proton spins. The relaxivity of water is low as the energy transfer between spins and lattice is inefficient. Increased *macromolecule* content in water will accelerate relaxation pathways in the solution via water-protein interactions (Jiao, Bryant 1996). Since *hemoglobin* is the dominant blood macromolecule, alterations in hematocrit level (HCT, percentage red blood cells in blood) will influence the relaxivity of blood (Silvennoinen, Kettunen & Kauppinen 2003a). Consequently, T_1 will be shortened with increased volume of red blood cells.

During pulmonary gas exchange, oxygen diffuses across the alveolar membrane into the lung capillary blood and initially dissolves into blood plasma as molecular oxygen. *Oxyhemoglobin* is *diamagnetic* and is formed when the oxygen molecule couples with haemoglobin. *Deoxyhemoglobin*, in contrast, is *paramagnetic* because of the high spin state of the heme iron and is formed when oxyhemoglobin releases its oxygen to the tissues. Both molecular oxygen and deoxyhemoglobin shorten T_1 while oxyhemoglobin does not have any effect on T_1.

2.4.3.2 Lung diseases

Lung diseases can often be identified from the signal in the MR-images due to an induced change in S_0 (Beckmann et al. 2002). An increase in lung S_0 due to solid lesions or infiltration of liquids is easily detectable, when long TEs are used to produce a dark background of healthy lung parenchyma. Emphysematous lungs have a decreased S_0 which can be visualized with ventilation or perfusion imaging or quantified with T_2* measurements (Olsson et al. 2007a).

Stadler *et al*. found a T_1 shortening in the lungs of patients with *fibrosis* and *emphysema* (Stadler et al. 2007). One possible explanation to the shortened lung T_1 lies in vascular rarefaction or a redistribution of blood within the effected lung parenchyma. Also, fibrotic tissue has increased collagen content and other extra-cellular matrix components which lead to an increased fraction of bound water that could shorten T_1. This is further supported by a study of rat lungs in which a significant shortening of T_1 in the fibrotic stage of lung injury was found (Vinitski et al. 1986).

All factors described in this subsection are summarized in Table 3 along with the expected changes on lung T_1 and T_2*.

Table 3. Effect of various factors and pathologies on lung T_1 and T_2*.

Increased	Expected changes in relaxation	
Factor/Pathology ↑	ΔT_1	ΔT_2*
O_2	↓	-
Hb	↓	↓
HbO_2	-	-
H_2O (Edema)	↑	↑
Macromolecule (Collagen, HCT)	↓	↓
Temperature	↑	↑
Lung volume	↓	↓
B_0	↑	↓
Fibrosis	↓	↓
Emphysema	↓	↓
COPD	↓	↓

O_2 – dissolved oxygen, Hb – deoxyhemoglobin, HbO_2 – oxyhemoglobin, B_0 – magnetic field.

2.5 T_1 measurement techniques

In order to measure T_1-maps, two or more series of images are acquired, each weighted slightly differently, to sample the recovery or decay of MR signal. The inversion recovery (IR) and variable flip angle (VFA) techniques are two of the most common T_1 measurements methods and were applied in this thesis.

2.5.1 The inversion recovery technique

The gold standard to assess T_1 is by IR acquisitions that offer accurate and precise T_1 measurements (Gowland 2003). The IR method is accurate since it does not rely on the application of a pulse with an accurately known flip angle (FA). For this reason, IR has served as the reference technique for 2D T_1 measurements both *in vivo* and in phantom studies throughout our work. The IR method begins with an inversion pulse separated by an inversion time (TI) to a SE readout. The inverted longitudinal magnetization (M_z) recovers exponentially at a rate described by T_1. The sampled recovery curve is fitted to the IR signal equation:

$$SI = S_0(1 - 2fe^{\frac{TI}{T_1}} - (1 - 2f)e^{\frac{nTE-TR}{T_1}}), \tag{2.1}$$

where SI = signal intensity, S_0 = signal expected without the application of an inversion pulse, f = inversion efficiency set to 1, and n = echo train length (Kingsley, Gordon Monahan 2001).

The whole last term in Eq. (2.1) is a constant and can therefore be written as

$$SI(TI) = A - Be^{TI/T_1}, \tag{2.2}$$

where $SI(TI)$ is the signal intensity at time TI, A is a constant for the offset and B is a constant for the S_0 (Kingsley, Gordon Monahan 2001).

However, IR acquisitions require relatively long scan times time as they require long TRs. Therefore, fast readouts following the inversion pulse have been proposed such as RARE, rapid acquisition with relaxation enhancement (**Paper III)** or even faster version of RARE, i.e. HASTE (**Paper I)**.

Another rapid IR readout is the snapshot FLASH (Fast Low Angle Shot) (**Paper II**), which measures T_1 from a single recovery of longitudinal magnetization (Jakob et al. 2001). The single inversion pulse is followed by a series of very small FA excitation pulses with GE readouts to sample the T_1 curve.

2.5.2 The variable flip angle technique

An approach towards rapid 3D T_1 mapping is to vary the FA of a spoiled GE or a UTE 3D acquisition. This method offers 3D T_1 mapping in less time than IR methods. T_1 quantification with the VFA technique uses two or more SPGRs applied with different FAs (Homer, Beevers 1985). The signal S from a SPGR imaging sequence is given by

$$S = M_0 \frac{1 - e^{-TR/T_1}}{1 - e^{-TR/T_1} \cos\alpha} \sin\alpha \tag{2.3}$$

where M_0 is the initial longitudinal magnetization, α is the FA of the RF excitation pulse and TR is the time between the RF pulses. For a narrow range of T_1 values a pair of measurements of two optimal FAs can be used for T_1 mapping (Wang, Riederer & Lee 1987) (**Paper III&IV**). For a large range of T_1 values at least three FAs should be acquired. By acquiring the same GE sequence twice, with all parameters equal except the FA, Eq 2.3 can be solved for T_1:

$$T_1 = \frac{\mathrm{TR}}{\ln\left(\frac{S_2 \sin\alpha_1 \cos\alpha_2 - S_1 \sin\alpha_2 \cos\alpha_1}{S_2 \sin\alpha_1 - S_1 \sin\alpha_2}\right)} \tag{2.4}$$

where S_1 , α_1, S_2 and α_2 are the signals and FAs of the first and second SPGR sequence, respectively.

This VFA method is sensitive, particularly at short TRs, to incomplete spoiling of the RF pulse leading to stimulated echoes and is also sensitive to inaccurate FA estimates particularly when T_1 values are long.

2.6 T_1 as a biomarker

For MR biomarkers, it is important to establish repeatability and variation, to determine how persistent the measured T_1 results are between successive examinations before investigating response to therapy. A biomarker is a characteristic that is objectively measured and evaluated as an indicator of normal biological processes, pathogenic processes or pharmacologic responses to a therapeutic intervention (Waterton 2013). Blood pressure and metabolites measured in blood or urine such as glucose and cholesterol are examples of biological biomarkers. Examples of *imaging* biomarkers assessed with MRI are: tumor size, myocardial infarct size with late gadolinium enhancement and T_2* in liver, a biomarker of iron overload.

2.6.1 Repeatability and reproducibility

For MRI biomarkers the concepts of repeatability and reproducibility overlap and are often wrongly applied in the literature. *Repeatability* or test–retest reliability is the variation in measurements on a single instrument on the same item, under the same conditions, and in a short period of time. The test should give the same result within a predefined standard deviation. *Reproducibility* is the ability of an entire experiment or study to be reproduced. The test conducted twice on comparable subjects, in different labs, using different equipment, by different operators, over different periods of time, by either the researcher or by someone else working independently should give comparable results.

2.7 Ultra-short echo time sequences

UTE sequences are suitable for imaging tissues with short T_2 or T_2*, such as the lungs. The TEs for UTE sequences are in the μs range, which is possible because of a short excitation pulse, radial k-space trajectory and gradient ramp sampling. The oversampling of the center of k-space results in enhanced SNR with reduced motion artifacts in comparison to Cartesian readouts (Figure 3).

The k-space trajectories may deviate from the ideal as UTE imaging sequences require fast gradient switching and ramping. These k-space deviations can be corrected by using the actual k-space trajectories for the reconstruction, which is performed by a separate trajectory measurement (Zhang et al. 1998). Before image reconstruction, the radial k-space data is interpolated and regridded onto a Cartesian grid (Figure 3). The Cartesian grid is corrected via a density weighting function for the oversampled radial data, prior to Fourier transformation. A total number of approximately $\pi \cdot (matrix\ size)^2$ evenly spaced spokes is required to fulfil the Nyquist criterion and to avoid aliasing artefacts in the reconstructed 3D image. Thus, if the k-space is more or less uniformly covered in data acquisition and the actual k-space trajectory is known, accurate image reconstruction can be achieved by regridded interpolation and Fourier transformation.

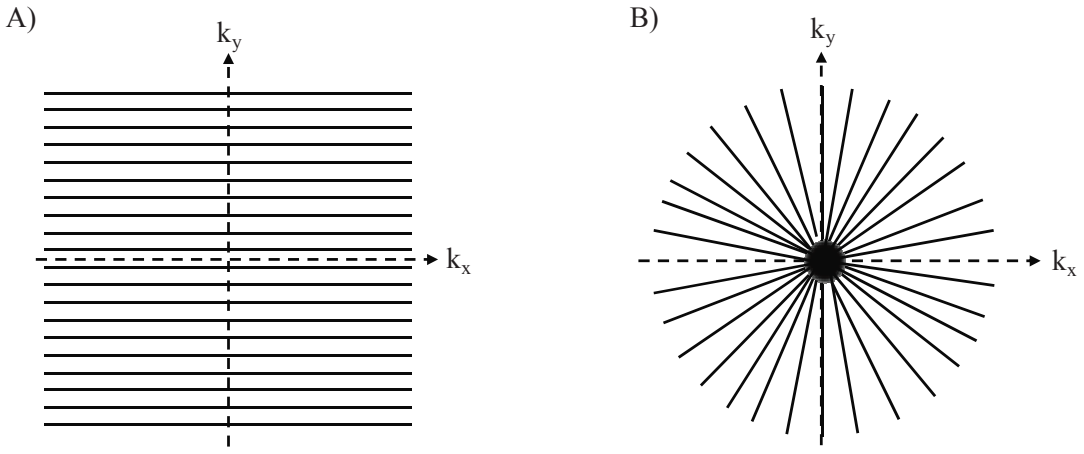

Figure 3. The k-space trajectories for (a) conventional Cartesian and (b) radial readouts. Note that the center of k-space with the low-frequency components are oversampled in the radial sequence, which provides signal averaging leading to artifact reduction.

3. Experimental results from simulations and *in vitro* measurements

3.1 Optimization of the VFA method for T_1 measurements

In this thesis a preclinical T_1 mapping protocol was developed in which two 3D-UTE images with different FAs were acquired. The aim was to perform a 3D T_1 map within 20 min. We optimized the T_1 sensitivity by finding the optimal FAs, repetition time (TR) and spatial resolution. The actual FA was calculated as the VFA technique is known to be sensitive to the FA eestimation. Finally, phantom measurements were performed to verify the accuracy and precision of the 3D-UTE T_1 measurement protocol.

There is a specific FA at which the signal from a SPGR sequence has a maximum (Eq. 2.3) for a given T_1 and TR, denoted as the Ernst angle. The FA combination for the 3D-UTE images was chosen for a signal, 71% of that at the Ernst angle (Figure 4). In house *in vivo* experiments indicated that the T_1 of mouse lungs at 4.7 T was approximately 1300 ms and therefore the optimal FAs were 3° (S_0 weighted FA) and 17° (T_1 weighted FA). The calculated T_1 will be least sensitive to any acquired noise with this FA combination (Deoni, Rutt & Peters 2003).

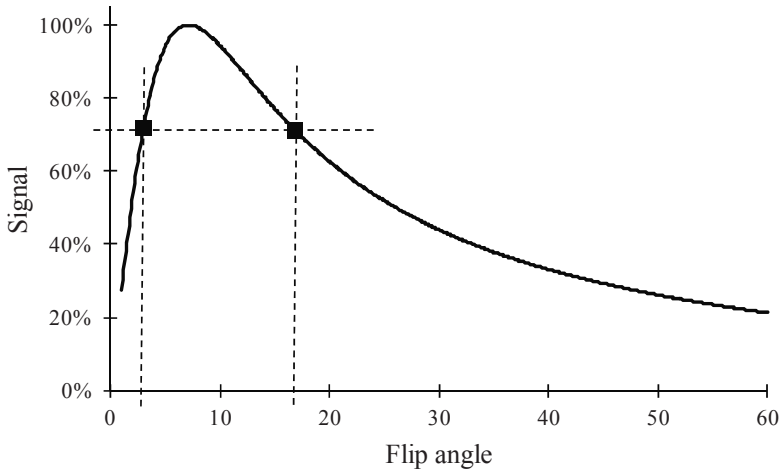

Figure 4. Spoiled gradient echo signal as a function of flip angle (Eq. 2.3), for a T_1 of 1300 ms and TR of 10 ms. The optimal variable flip angle combination is 3° and 17° for these parameters, marked with squares.

A numerical simulation was performed in order to determine the precision of the sequence's T_1 assessment at different TR values. Each simulation included 100,000 estimates, with the T_1 for each run being calculated according to the SPGR equation (Eq. 2.3). Random noise was added to the signal with one standard deviation. The mean T_1 was calculated as the inverse of the average value of the simulated $1/T_1$ in order to avoid bias in the assessment.

The precision of T_1 was optimized for a fixed total scan time and fixed T_1, so that for decreasing TR/T_1, the number of signal averages allowed increases. The simulated standard deviation and relative standard deviation (standard deviation/mean) of T_1 versus TR/T_1 is illustrated in Figure 5. It can be seen that the T_1 precision reduces with increased TR/T_1 ratio. The simulation shows that it is better to use short TRs and average the signal over a longer scan time instead of spending the time for long TRs. Therefore, we used a TR of 10 ms together with a matrix size of 140^3, which resulted in a total acquisition time of 20 min for the two FAs acquired with 3D-UTE. A shorter TR would reduce SNR and change the first optimal FA to 2°, which might be hard to accurately acquire as the accuracy of the FA values is degraded with very small RF amplifier output (Schabel, Morrell 2009).

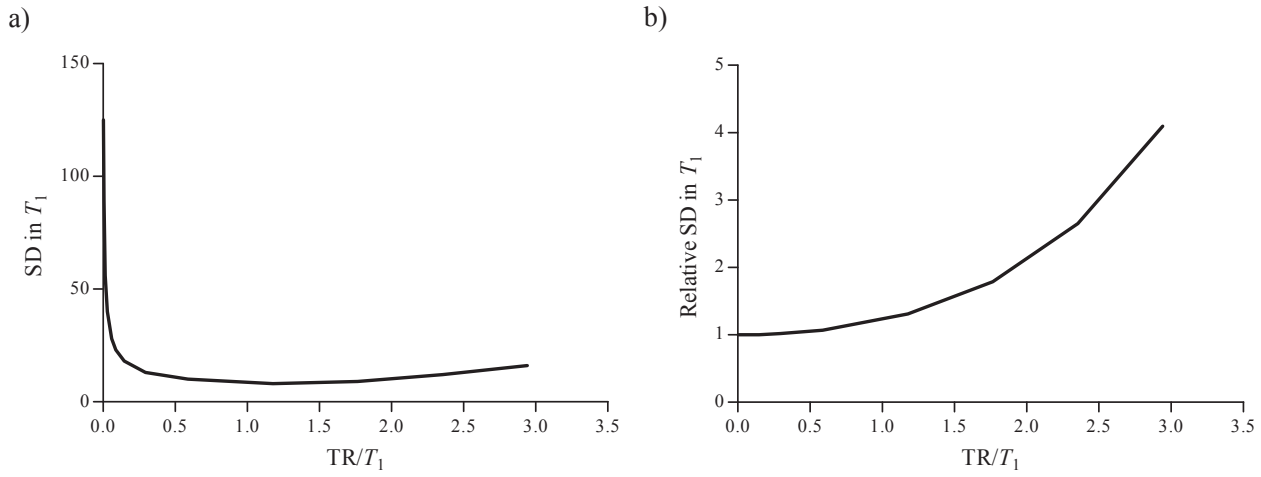

Figure 5. Plots of the a) standard deviation and relative standard deviation (standard deviation /mean) versus TR/T_1 using the optimum two FAs for a fixed T_1 and fixed total scan time, assessed via numerical simulations. The plots show that short TRs and averaging the signal was better than spending the time for long TRs.

3.1.1 Calculation of flip angle

Knowledge of the *actual FA* is necessary for T_1 quantification. The real FA of the 3° S_0 weighted scan was calculated using a FLASH 3D with the phase encoding gradient turned off and the same parameters as for the *in vivo* experiments (**Paper III&IV**). A spherical phantom with water, long T_1, was placed in the isocenter.

If consecutive signals after each RF pulse are acquired with identical acquisition parameters, i.e. constant FA, the ratio of the signal intensity S_1 within a region of interest (ROI) of an image to that of the intensity S_0 within the identical ROI in the previous signal can be expressed by:

$$S_1 = S_0 \cos\alpha,$$

where S_1 is the longitudinal magnetization signal after one RF pulse of FA α (Markstaller et al. 2000).

Assuming that the T_1 relaxation during the measurement can be neglected (TR<<T_1) the signal in the read direction will decay due to the RF-pulse train. The longitudinal magnetization signal, S_0, will reduce due to the RF pulses in the following way:

After the next RF pulse:

$$S_2 = S_1 \cos\alpha = S_0 \cos\alpha \cos\alpha = S_0 \cos^2\alpha$$

and after n pulses:

$$S_n = S_0 \cos^n\alpha$$

using natural logarithms

$$\ln\frac{S_n}{S_0} = \ln\cos^n\alpha = n \ln\cos\alpha$$

$$\ln\frac{S_n}{S_0}/n = \ln\cos\alpha$$

$$\exp\left[\ln\frac{S_n}{S_0}/n\right] = \cos\alpha$$

$$\alpha = \cos^{-1} \exp\left[\ln \frac{S_n}{S_0}/n\right] \tag{3.1}$$

If the logarithms of the signals are plotted over the number of RF pulses, the slope of the straight line will be in the right hand side of the expression above (slope = $\ln[S_n/S_0]/n$) (Figure 6). The FA can be calculated from $\cos^{-1} \exp[slope]$, where the slope is calculated from the linear regression of number of RF pulses versus the measured logarithmic values of the signals.

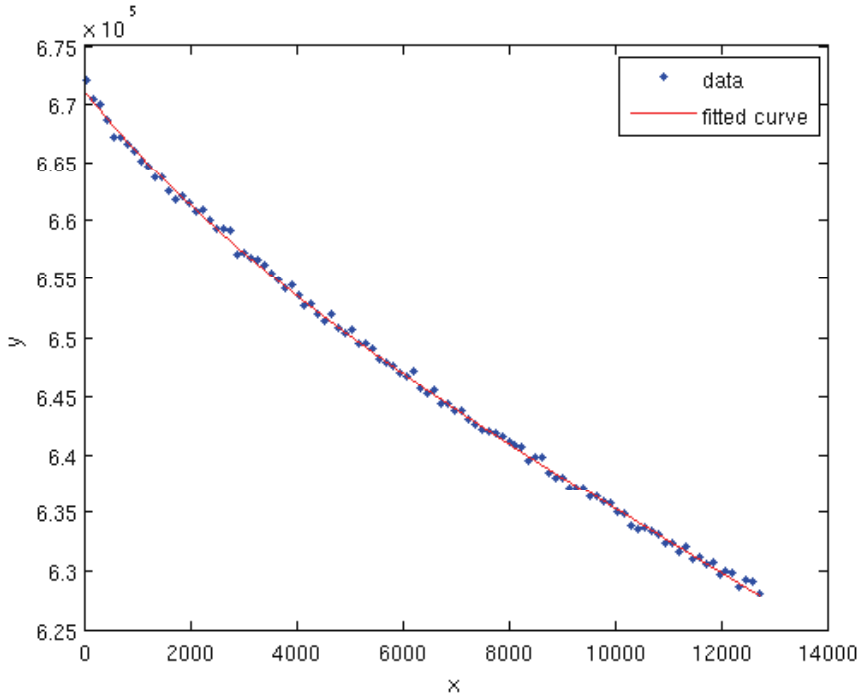

Figure 6. The decay of the signal due to the train of RF-pulses. The FA can be calculated from the fitted line. In this particular measurement FA 3° was estimated.

In this work, we found less than 5% FA error on FA 3° and no correction of the T_1 quantification was performed (**Paper III&IV**).

3.1.2 Accuracy and precision of T_1

Phantom measurements were performed to verify the *accuracy* and *precision* of the 3D-UTE T_1 measurement protocol (**Paper III**). Figure 7 compares T_1 measured with VFA 3D-UTE and an IR-RARE sequence for phantoms with different T_1 values. The agreement of the sequences was found to be very good with a Pearson's correlation coefficient of 0.99 ($p<0.0001$).

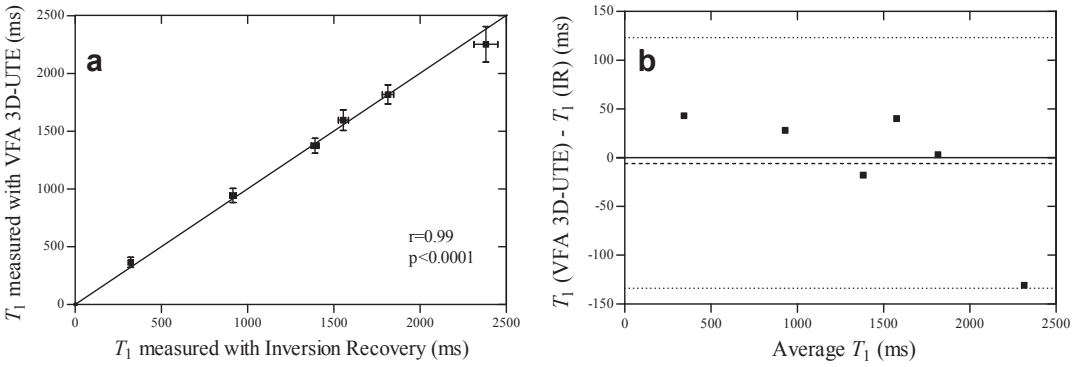

Figure 7. Comparison of phantom T1 values measured with VFA 3D-UTE and Inversion recovery a) through Bland-Altman plot b) showed good agreement (Paper III). The dotted lines represent mean ± 2 SD (**Paper III**).

The optimized VFA 3D-UTE protocol provided accurate FAs, which led to accurate and precise T_1 values in phantoms within 20 min (Table 4). The next step was to test the protocol *in vivo* (section 4.2).

Table 4. Acquisition parameters for the 3D-UTE sequence.

TR	10 ms
TE	8 μs
FOV	40x40x50 mm^3
Matrix	140^3
FA	3°, 17°
Radials	61,214

3.2 Simulation of blood T_1 in the hypoxic regime

The concentration of oxygen in the blood is usually described as the PaO_2, which easily is measured with a blood test. PaO2 is also used to reflect the alveolar partial O_2 pressure (pO_2) in the lung tissue. Inhalation of elevated oxygen concentrations will increase alveolar pO2 and consequently the plasma PaO_2 because of the dissolved oxygen, which also will shorten the T_1. This linear relationship with increased R_1 ($1/T_1$) for higher PaO2 in the lung is well known (Hatabu et al. 2001). However, the correlation of lung T_1 vs. PaO_2 in less oxygenated areas has not been described in detail.

Therefore, we performed a simulation between lung R_1 and PaO_2 with oxygen pressures lower than the normal level 100 mmHg. This hypoxic regime will increase our knowledge of how blood R_1 might alter areas of the lung affected by a disease. A modified version of Hill's equation (Severinghaus 1979a) was used to calculate the saturation of oxygen in blood for varied partial O_2 pressure values. This equation describes the human blood oxygen dissociation curve at 37 °C:

$$S = ((23{,}400((pO_2)^3 + 150pO_2)^{-1}) + 1)^{-1} \quad (3.2)$$

where S is the saturation of oxyhemoglobin and pO_2 is the partial pressure of oxygen. The hemoglobin concentration in blood was assumed to 15g/100 ml blood, i.e. the normal value for man (Nordin et al. 2004). Henry's law was applied for the dissolved oxygen concentrations. A constant of 0.031 ml dissolved oxygen per liter blood was used (Severinghaus 1979b, Haddock et al. 2013).

The simulation showed that R_1 in blood shortens with lower PaO_2 down to moderate hypoxia of around 40 mmHg (Figure 8). R_1 stabilizes with lower PaO_2 for serious hypoxia, <40 mmHg. For patients with COPD the PaO_2 is decreased and may vary from 76 mmHg for moderate (GOLD II) to 61 mmHg for severe COPD (GOLD IV) (Skjørten et al. 2013). Figure 8 also shows a reduced deoxyhemoglobin concentration in blood with increased PaO_2 due to saturation of oxyhemoglobin.

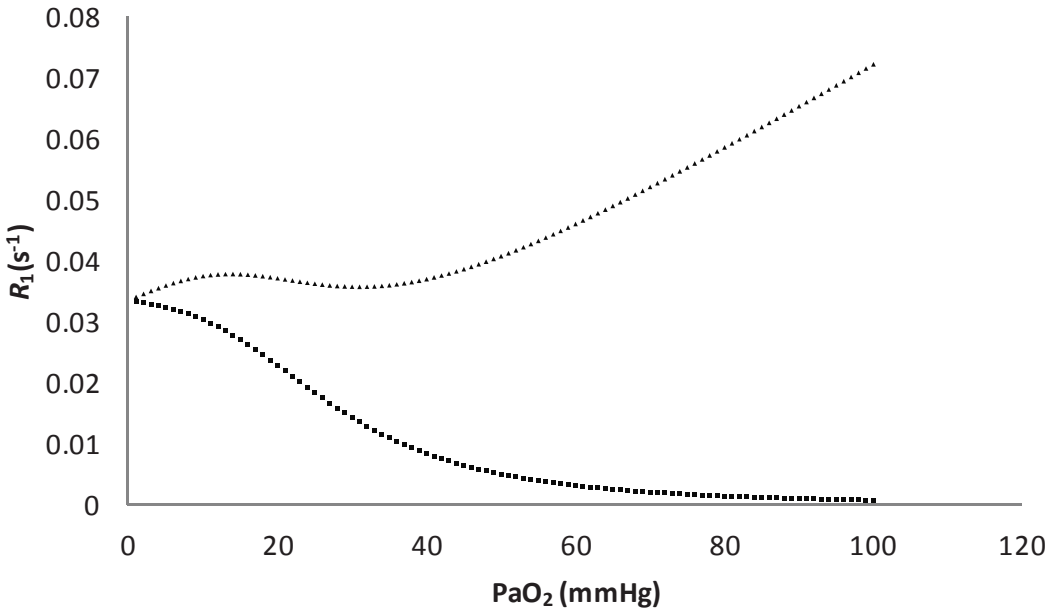

Figure 8. Simulated relationship between R_1 ($1/T_1$) in blood (▲) and deoxyhemoglobin (■). The plot shows that R_1 in blood stabilizes in the hypoxic regime.

3.3 Tobacco smoke effect on T_1 measured in gadolinium doped water

Up to 5000 different substances including metals, such as nickel, have been identified in fresh TS (Kilburn 1984). TS is an aerosol consisting of solids and liquid droplets in a gaseous phase. The presence of these substances, metals or tar could enhance dipolar relaxation in the extracellular tissue water which accumulates in the lung as a direct consequence of smoking. In order to test this hypothesis T_1 measurements on cigarette smoke extract (CSE) was performed in our laboratory.

The CSE was prepared according to a previous report (Edirisinghe et al. 2008). Mainstream smoke of 0, 1, 5 and 10 cigarettes **(**Research grade cigarettes (3R4F), Kentucky Tobacco Research & Development Center, University of Kentucky, Lexington, Kentucky**)** without filter was withdrawn steadily via a pump and the smoke was purged in 20 ml of gadolinium doped water (Figure 9.). Subsequently, the CSE was poured into small plastic vials and then scanned on a 4.7 T MRI scanner. T_1 measurements were performed with both 2D IR-RARE and VFA 3D-UTE. No significant T_1 changes were observed in the CSE compared to control samples.

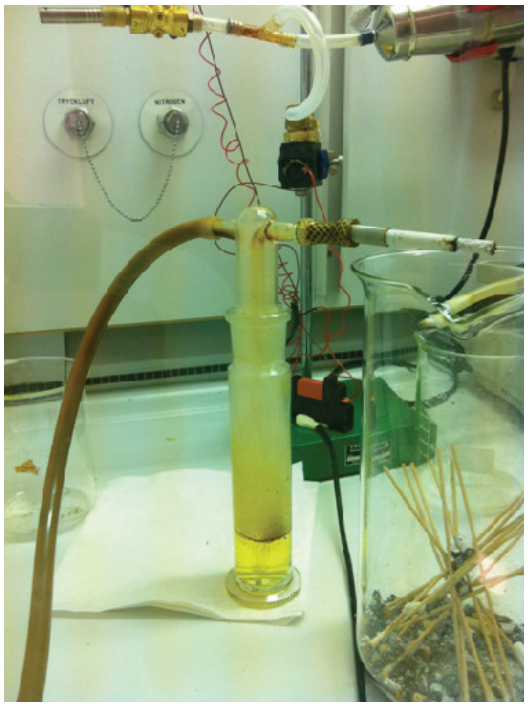

Figure 9. Preparation of cigarette smoke extract.

4. Results from i*n vivo* T_1 measurements in man and mice

This thesis is based on four *in vivo* studies, two in humans and two in mice. First, we investigated if lung T_1 can be used as a biomarker of COPD in man (**Paper I**). Second, we investigated whether there is a direct effect of TS exposure on lung T_1 in healthy current smokers (**Paper II**). Third, MR imaging of small animals was performed, in order to increase the understanding of how T_1 relates to the underlying pathophysiology of COPD. A 3D-UTE protocol for T_1 measurements in mice was developed (**Paper III**), to enable a COPD study in mouse (**Paper IV**).

4.1 Lung T_1 measurements in COPD patients and healthy smokers

COPD patients were studied with a conventional robust T_1 method in correlation to other relevant markers (**Paper I**) (Alamidi et al. 2015). Subsequently, as tobacco smoking is a major risk factor for development of COPD, healthy current smokers with no known lung disease and age matched never smokers were examined (**Paper II**).

4.1.1 Repeatability of lung T_1

A repeatability study was performed to investigate the potential of lung T_1 mapping as a biomarker of COPD. Prior to this work, only one study had performed a lung T_1 repeatability study in 12 subjects (Renne et al. 2015). We examined 27 subjects twice with a one-week interval, using the same free breathing IR T_1 protocol at both occasions (**Paper I**). The median lung T_1 of each subject was satisfactorily repeatable between visits with an intraclass correlation coefficient (ICC) of 0.72. The mean T_1 difference and CV assessed from the median T_1 maps obtained from the two visits were 5 ms and 2.5%, respectively (Figure 10). Thus, T_1 values were averaged for each individual across the two scanning visits before testing for significant group differences and correlations.

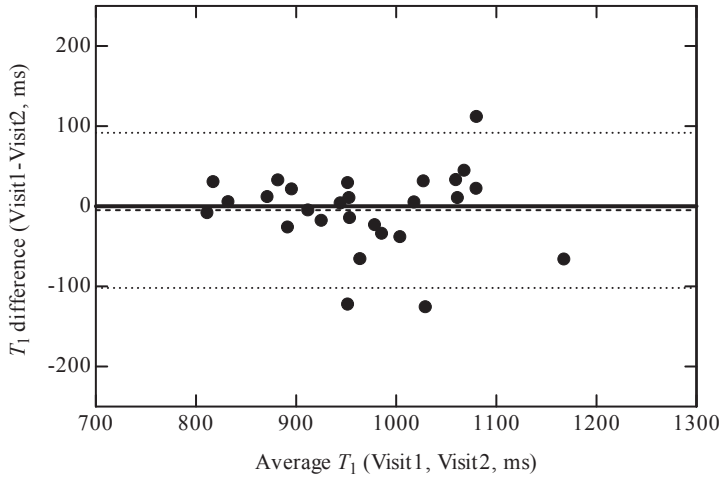

Figure 10. Mean lung T_1 from two repeated scans in one week plotted against their difference according to Bland-Altman analysis (**Paper I**). The dotted lines represent mean ± 2 SD.

4.1.2 Lung T_1 shortening in COPD patients

All COPD subjects were current or former smokers and had reduced lung function assessed by PFTs (**Paper I**). They were divided into two groups; moderate COPD, defined by FEV_1 > 50% predicted and severe COPD group FEV_1 < 50% predicted. The lung T_1 (mean ± SD) was significantly shorter (10%, $p<0.0001$; 14%, $p<0.0001$) for the moderate COPD subjects (947 ± 56 ms) and severe COPD subjects (911 ± 64 ms) than in the healthy controls (1053 ± 55 ms) (Figure 11).

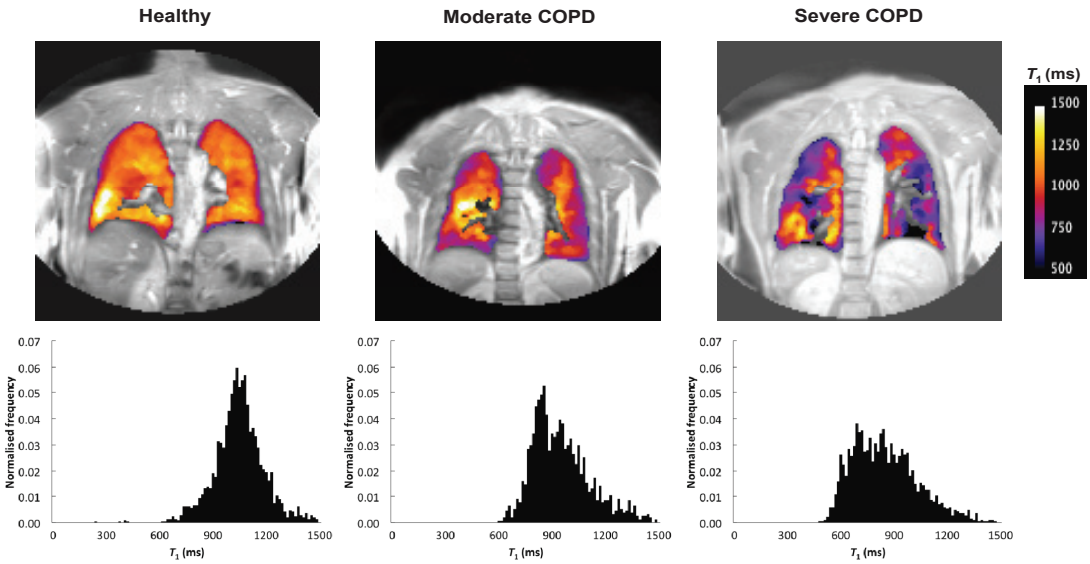

Figure 11. Representative coronal lung MRI T_1 maps overlaid on a signal intensity image with corresponding normalised T_1 histograms for healthy, moderate COPD and severe COPD subjects. Both T_1 maps and histograms reflected the severity of COPD by reduced T_1 and increased heterogeneity (**Paper I**).

4.1.3 T_1 correlation to CT and PFT measurements in COPD patients

All subjects underwent PFTs, whereas only the COPD patients were scanned using CT to allow quantification of lung density (**Paper I**). Strong significant correlations ($p<0.0001$) between lung T_1 and all PFT measurements were observed. Lung T_1 significantly ($p<0.01$) correlated with lung density assessed with CT.

4.1.4 Shortening of lung T_1 with age in healthy subjects

In the second work, performed in healthy subjects, lung T_1 was shortened with age but was not affected by pack-years (number of years or equivalent years in which 20 cigarettes a day was smoked, PY) in healthy smokers (Figure 12) (**Paper II**). Following compensation for age, PY did not reach statistical significant correlation to T_1, although it was close to significance, $p=0.08$.

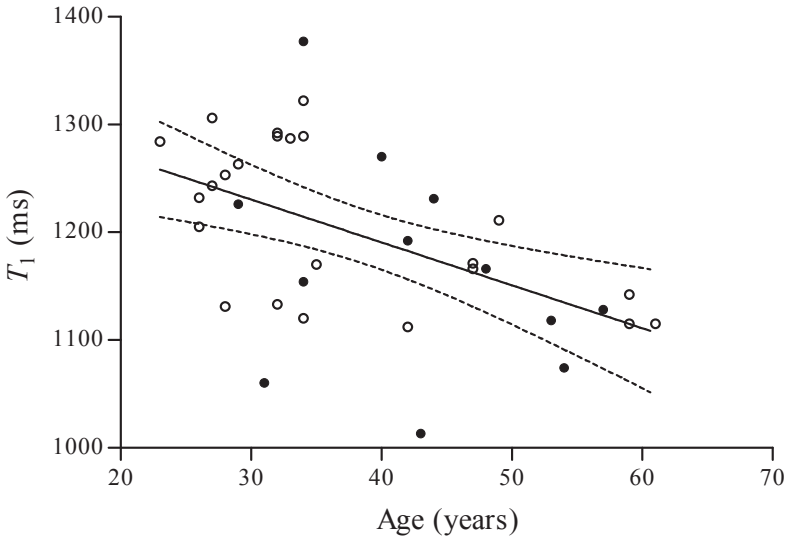

Figure 12. Lung T_1 as a function of age for smokers (●) and non-smokers (○). Significant ($p<0.01$) correlation between lung T_1 and age was found (**Paper II**).

4.2 VFA 3D-UTE measurements in naive mice and in an animal model of COPD

Initially, a conventional cardio-respiratory gated IR-RARE method was developed for T_1 measurements in freely breathing rodents (Alamidi 2010). However, the protocol was restricted to 2D imaging, relatively long TE and an advanced respiratory gated setup. To enable signal from lung parenchyma and quantify whole lung T_1 in free breathing rodents a radial VFA 3D-UTE method with ultra-short TE, 8 μs, was implemented (**Paper III**). This method provided accurate and precise T_1 measurements in phantoms (section 3.1.2).

Preceding in house *in vivo* experiments with multiple FAs indicated a T_1 in mouse lungs of approximately 1300 ms. Accordingly, the two optimal FAs were set to 3° - S_0 weighted FA and 17° - T_1 weighted FA, i.e. ~71% of the signal measured at the Ernst Angle (Deoni, Rutt & Peters 2003). T_1 maps were calculated by fitting the SPGR signal equation (Eq. 2.3) pixel-by-pixel over the two lung images for each slice using a self-developed Matlab script (MatlabR2013a; Mathworks, Natick, MA, USA). The whole lungs were segmented with a semi-automatic method, in which a region based active contour algorithm (Lankton, Tannenbaum 2008) was defined in order to extract the lungs from the image. Representative 3D-UTE lung images with corresponding T_1 maps of one animal are shown in Figure 13.

Finally, the 3D-UTE T_1 protocol was applied in a murine model of COPD together with functional and biological measurements (**Paper IV**). The purpose was to explore the potential of 3D T_1 mapping for the assessment of regional lung disease in mouse.

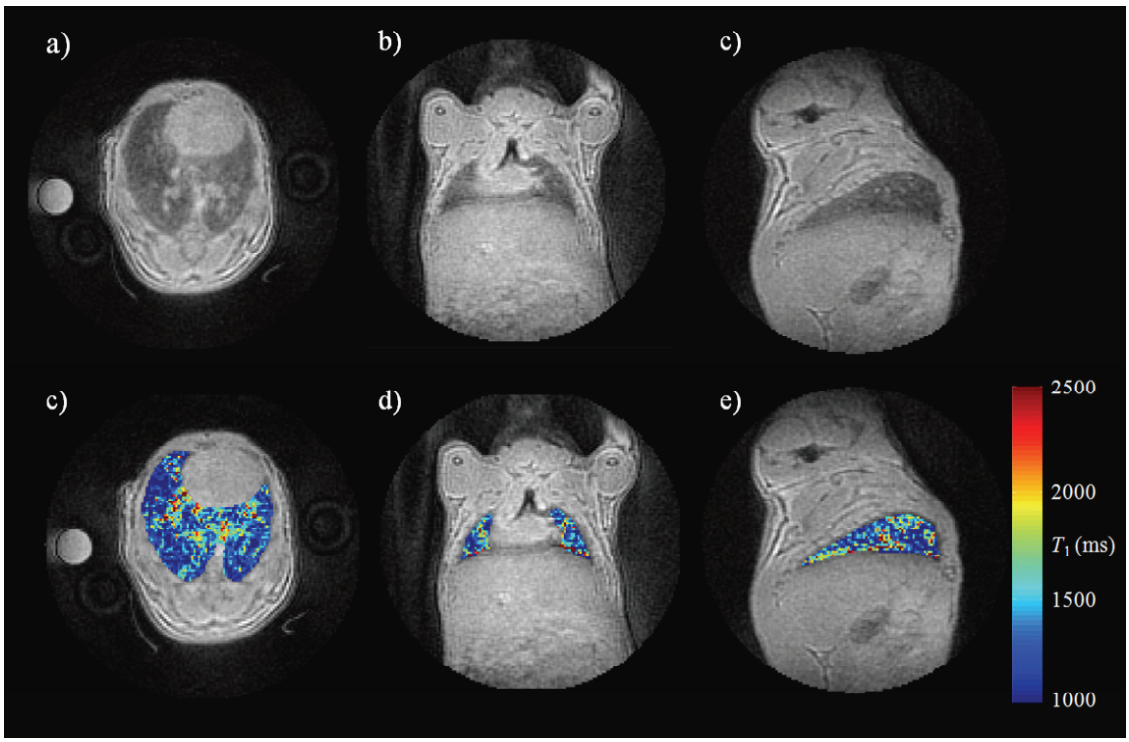

Figure 13. Axial, coronal and sagittal images from 3D UTE on a naive mouse together with T_1 maps overlaid on the images.

4.2.1 Repeatability of T_1 and S_0 in healthy mice lungs and muscle

Prior to this work, no rodent 3D lung T_1 mapping study had been performed. Therefore, our aim was to assess repeatability of T_1 and S_0 with our VFA 3D-UTE protocol to prove the concept that lung T_1 is suitable for therapy monitoring in mouse. Two experiments were performed (Figure 14). In experiment one, the inter-session repeatability of T_1 and S_0 measurements of both whole lung and muscle plus lung volumes was estimated by scanning the animals five times over one month. In experiment two, a second T_1 measurement was added to the imaging session at week number two in order to make an intra-session comparison.

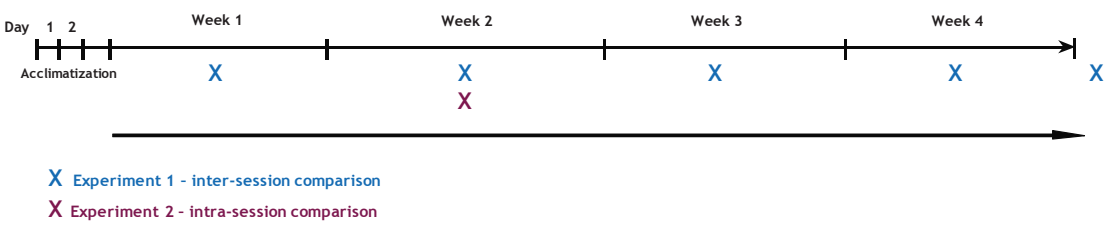

Figure 14. Schematic of the time schedule for MRI scanning of the mice (**Paper III**).

4.2.1.1 Experiment 1 – inter-session comparison

The overall mean T_1 assessed in lung and muscle in all animals over a month showed a 5% and 3% coefficient of variation (CV) (mean T_1 ± SD, 1255 ± 63 ms and 1432 ± 42 ms) (Figure 15). There were no significant differences in T_1 and lung volume between imaging sessions.

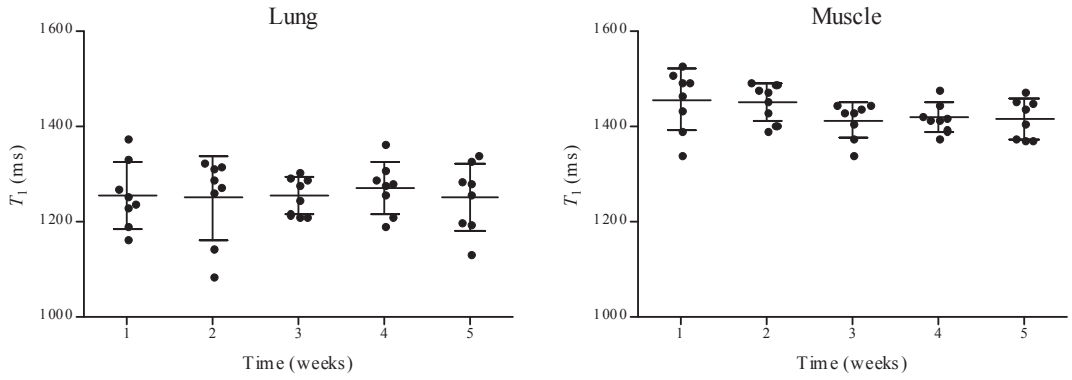

Figure 15. T_1 measurements over a month showed very good repeatability in lung and muscle with the VFA 3D-UTE method (**Paper III**). Data are means ± SD.

4.2.1.2 Experiment 2 – intra-session comparison

Mean lung T_1 and S_0 increased by 2% in the second intra-session scans (all $p<0.05$) (Figure 16). The lung volume decreased by 4% ($p<0.01$), the lung SI of the S_0-weighted FA 3° image increased by 4% ($p<0.05$) and no significant changes in muscle T_1 and S_0 were found.

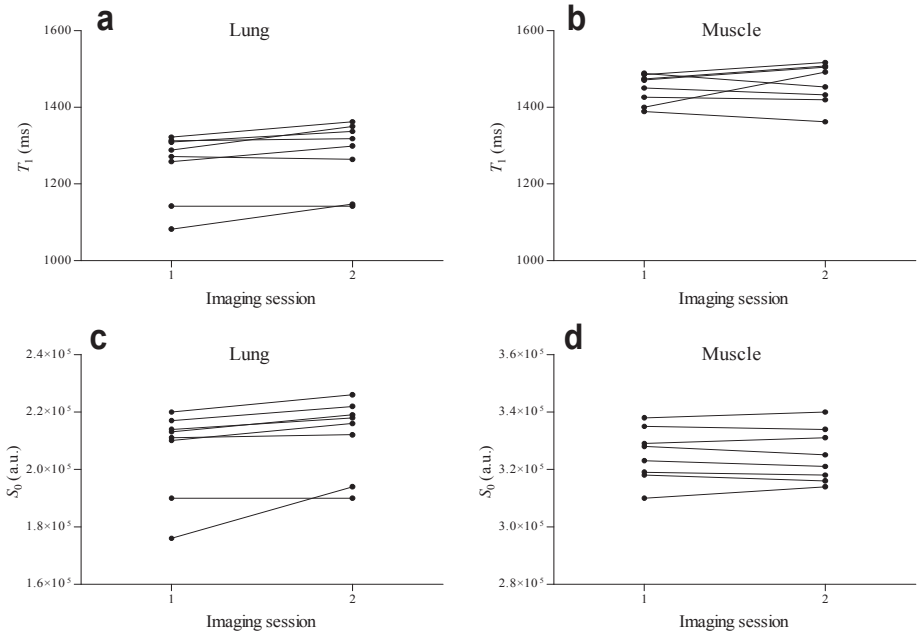

Figure 16. 3D-UTE T_1 repeatability in mouse lung and muscle during the same imaging session showed 2% increase in lung T_1 a) and lung S_0 c) ($p<0.05$) and no significant changes in muscle T_1 b) and muscle S_0 d) (**Paper III**).

4.2.2 T_1 measurements in an animal model of COPD

Lung T_1 measurements of TS exposed and control mice were performed weekly during one month to investigate T_1 as readout of a COPD mouse model (Figure 17). For the TS exposed mice, significant T_1 shortenings were found between baseline and two ($p<0.001$) and three ($p<0.001$) weeks exposure and between first and third ($p<0.05$) week (Figure 18). Significant T_1 increase was found between third and fourth week. No significant T_1 changes were observed in the control mice at any time point.

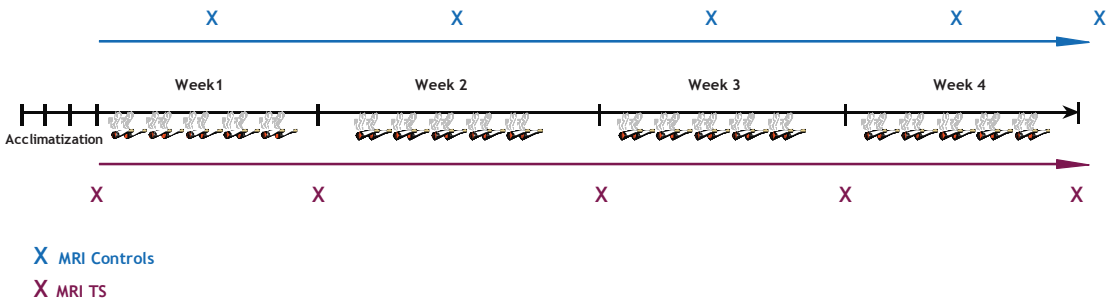

Figure 17. Schematic of the MRI scanning and TS exposure of the mice (**Paper IV**).

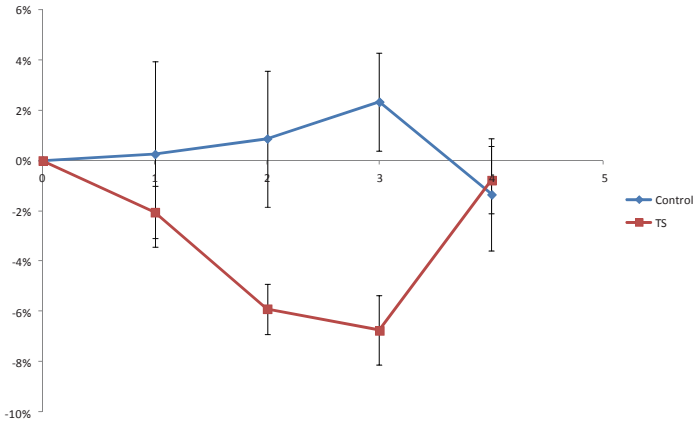

Figure 18. Mean lung T_1 change normalized to baseline for control and TS exposed mice. Data are presented as mean ± SD (**Paper IV**).

5. Discussion and conclusions

There is a need in drug discovery and pulmonary research to evaluate early phase of COPD with a sensitive, non-invasive, radiation-free and translational imaging method. A method that fulfills these conditions can facilitate clinical trials in drug development, benefit diagnosis and thereby profit patients from advancements in this field of research. In this thesis, the first steps have been taken to develop such a translational imaging method. MRI-based T_1 mapping shows potential as a repeatable, non-invasive, radiation-free and translational lung biomarker of COPD.

In four papers and additional experiments presented in this thesis the T_1 relaxation time of the lung has been studied. The main result, i.e. the finding that T_1 was shortened in COPD patients, most likely reflected smoking-induced lung pathology, specifically emphysema. This was supported by our PFT and CT measurements (**Paper I**). However, all COPD subjects examined in the study were current or former smokers. Therefore, it could be of concern that the T_1 shortening was an effect of the disease as well as an effect of accumulation of tar or other substances as a direct consequence of smoking. To test this hypothesis an investigation in healthy smokers was performed where we examined whether PY influenced lung T_1 per se (**Paper II**). In addition, samples with CSE was prepared and measured in the MR scanner (section 3.3) to test if potential paramagnetic tobacco particles could affect T_1. We were not able to detect a direct effect of tobacco smoke exposure on T_1 in healthy smokers ($p=0.08$) and no change of T_1 was found in the smoke samples. In the animal study, however, significant T_1 shortening in TS exposed mice was found (**Paper IV**).

Altogether, this leads to the conclusion that there is no effect on T_1 from the smoke alone. It is the effect of the smoke to the tissue leading to early damage and eventually a disease which is of importance, both in humans and animals. The healthy smokers, as defined by PFTs, may have small damage to the lungs induced by the smoke, but not the extent that there is a manifested disease. This reasoning is supported by the tendency to a significant relationship between T_1 and PY. Measurement of T_1 in a larger smoking but healthy cohort would increase the possibility to find a possible T_1 relationship to PY. Accordingly, it is only when the damages from the smoke are sufficiently large or a disease such as COPD is manifested, when a

significant effect on lung T_1 is found. In a study using an MR imaging technique with no potential relationship to the smoke itself, it was also concluded that the lung structure was damaged in healthy smokers with a similar smoking history to this study (Fain et al. 2006).

Even though there was no significant relationship between smoke exposure and T_1 four our study design, we did find that lung T_1 shortens with age in healthy subjects. Reduced blood hematocrite levels, reduced perfusion, decreased lung volume and increased macromolecular collagen content are all causes that could reduce T_1 in the ageing process of the lung. On the basis of our results, age can be a significant confounding factor when T_1 is used as a biomarker in lung MRI studies that must be taken into account to detect underlying patterns of disease.

The main application for lung T_1 mapping would be in clinical trials where there are needs to perform multiple scans and ionizing radiation would be a limitation. However, immediate application to clinical practice needs to be further justified.

Lung T_1 needs to be properly validated and qualified as there are difficulties in determining the exact physiological processes that have an effect on T_1 in the present COPD animal model. The lipopolysaccharide model of lung inflammation, which has a more pronounced acute inflammation than the TS model, could help to understand the inflammatory aspects of the change of lung T_1.

It is important not only to make an accurate diagnosis of COPD in patients who already have a deteriorated lung function and in those who are symptomatic but also in those patients who have an early or mild disease. MRI is of particular interest for the functional evaluation of patients with COPD. OE-MRI provides regional lung function, and if quantified by T_1 measurements the intrinsic T_1 values are also available. Notably, the functional information from OE-MRI for the same cohort as in **Paper I**, does not reveal more insight on the patient characteristics (Hubbard et al. 2011). Moreover, the proton density values, S_0, can be retrieved from the T_1 mapping that may provide extra information on the underlying biology. Lung T_1 and S_0 mapping could potentially distinguish between lung inflammation and fibrosis which is important for diagnosis and characterization of disease.

Despite large advances in this field, there is a need to establish a standard protocol that can be used and compared at different centers. This standardized protocol could include OE-MRI together with T_1 and S_0

assessments and proper image analysis. Thus, radiation-free lung MRI T_1 alone or together with S_0 and functional OE-MRI quantification is of considerable interest as an assessment of early COPD, especially for longitudinal studies.

Many of the limitations of this study are related to technical shortcomings. One could expect that the rapid technical development to the scientific applications of MRI will enable more accurate and faster acquisition of T_1 in the future. Accordingly, there will be room for improvements with studies of alternative designs in both man and animals to further validate the utility of MR T_1 mapping in the assessment of COPD.

5.1 Conclusions

The potential of MRI-based T_1 mapping to evaluate early COPD has been enhanced by the new knowledge presented in this thesis.

1. Lung T_1 mapping is an attractive imaging biomarker of COPD in man and mouse and suited for future longitudinal studies (**Paper I&IV**).
2. There is no direct effect of TS exposure on T_1 in healthy smokers (**Paper II**).
3. Lung T_1 shortens with age (**Paper II**).
4. VFA 3D-UTE provides accurate and repeatable T_1 mapping of the lung in mice and is therefore suitable to evaluate potential new medicines (**Paper III**).

6. Acknowledgements

First and foremost, I would like to express my deepest gratitude to my main supervisor Prof. Lars E. Olsson for your endless support, intellectual guidance and encouragement. You have been an excellent mentor and I have really appreciated working with you.

I would like to thank to Dr. Kerstin Lagerstrand, my co-supervisor, for always making time to fruitful and energetic discussions.

I am very grateful to Dr. Paul Hockings, my second co-supervisor, for your fantastic patience and engagement in our project and always finding time to help me.

I would like to thank my closest both former and current colleagues/coworkers/friends at AstraZeneca: Abdel Bidar for your warm enthusiasm and friendly support, Dr. Amir Smailagic for your trust and our exciting discussions, Mikael Bengtsson for being a king friend and 24/7 Linux support, Dr. Frank Risse for pushing me on my science and German skills, Dr. Linda Swedin for being a sweet colleague and friend, Dr. Lars Nordenmark for effective collaboration, Jelena Pesic for sharing your lab tricks, Dr. Edvin Johansson for interesting theoretical discussions and Dr. Malin Gustavsson for you lab support. I also want to thank Dr. Leif Hultin, Dr. Anastassia Karageorgis, Nicole Parker, Dr. Marita Olsson, Dr. Sonya Jackson, Dr. Yazdan Shirvany, Dr. Christina Fakt, Lena Palm-Persson, Dr. Sally-Ann Emmas, Dr. Simon Young and the staff at LAS facility - especially Marita Pettersson.

Thank you all in Manchester: Dr. Geoff Parker, Dr. Penny Hubbard Cristinacce, Dr. Josephine Naish, Niall Maguire and Dr. John Waterton for a successful collaboration. Special thanks to Dr. Alexandra Morgan, my co-author, for a great teamwork.

Many thanks to the radiation physics group in Malmö for your kind welcome and particularly my coauthor Simon Kindvall.

I am thankful to the MR physics group at Sahlgrenska for showing interest in my project.

I would like to thank Svensk förening för radiofysik for funding my travels and Pinet for exciting lung workshops and networking.

Thanks Sjukhusfysikermaffian – My brusch Emil, Johan, Förnvik, Sicko, Stoffe – you guys are amazing.

Last but not least, my warmest thanks to my family for always being there for me and for giving me the best conditions to do what I want in life. Mamma, Pappa, David and Babcia. Love you!

7. References

Agustí, A. 2013, "Phenotypes and disease characterization in chronic obstructive pulmonary disease. Toward the extinction of phenotypes?", *Annals of the American Thoracic Society,* vol. 10, no. Supplement, pp. S125-S130.

Alamidi, D., Morgan, A., Hubbard, P., Nordenmark, L., Hockings, P., Lagerstrand, K., Young, S., Naish, J., Waterton, J., Maguire, N., Olsson, L.E. & Parker, G.J. 2015, "COPD patients have short lung magnetic resonance T_1 relaxation time", *COPD: Journal of Chronic Obstructive Pulmonary Disease*. In press.

Alamidi, D. 2010, "Lung imaging using oxygen-enhanced MRI in small animals", *MSc Thesis,* .

Armstrong, J.D., Gluck, E.H., Crapo, R.O., Jones, H.A. & Hughes, J.M. 1982, "Lung tissue volume estimated by simultaneous radiographic and helium dilution methods", *Thorax,* vol. 37, no. 9, pp. 676-679.

Ashraf, H., Lo, P., Shaker, S.B., de Bruijne, M., Dirksen, A., Tønnesen, P., Dahlbäck, M. & Pedersen, J.H. 2011, "Short-term effect of changes in smoking behaviour on emphysema quantification by CT", *Thorax,* vol. 66, no. 1, pp. 55-60.

Bankier, A.A., O'Donnell, C.R., Mai, V.M., Storey, P., De Maertelaer, V., Edelman, R.R. & Chen, Q. 2004, "Impact of lung volume on MR signal intensity changes of the lung parenchyma", *Journal of Magnetic Resonance Imaging,* vol. 20, no. 6, pp. 961-966.

Barth, M. & Moser, E. 1997, "Proton NMR relaxation times of human blood samples at 1.5 T and implications for functional MRI", *Cellular and molecular biology,* vol. 43, pp. 783-792.

Bauman, G. & Eichinger, M. 2012, "Ventilation and perfusion magnetic resonance imaging of the lung", *Polish Journal of Radiology,* vol. 77, no. 1, pp. 37.

Bauman, G., Puderbach, M., Deimling, M., Jellus, V., Chefd'hotel, C., Dinkel, J., Hintze, C., Kauczor, H. & Schad, L.R. 2009, "Non-contrast-enhanced perfusion and ventilation assessment of the human lung by means of fourier decomposition in proton MRI", *Magnetic Resonance in Medicine,* vol. 62, no. 3, pp. 656-664.

Beckmann, N., Tigani, B., Sugar, R., Jackson, A.D., Jones, G., Mazzoni, L. & Fozard, J.R. 2002, "Noninvasive detection of endotoxin-induced mucus hypersecretion in rat lung by MRI", *American journal of*

physiology.Lung cellular and molecular physiology, vol. 283, no. 1, pp. L22-30.

Bergin, C., Müller, N., Nichols, D., Lillington, G., Hogg, J., Mullen, B., Grymaloski, M., Osborne, S. & Pare, P. 1986, "The diagnosis of emphysema. A computed tomographic-pathologic correlation.", *The American Review of Respiratory Disease,* vol. 133, no. 4, pp. 541.

Biederer, J., Beer, M., Hirsch, W., Wild, J., Fabel, M., Puderbach, M. & Van Beek, E.J. 2012, "MRI of the lung (2/3). Why… when… how?", *Insights into imaging,* , pp. 1-17.

Biederer, J. 2005, "[Magnetic resonance imaging: technical aspects and recent developments].", *Medizinische Klinik (Munich, Germany: 1983),* vol. 100, no. 1, pp. 62-72.

Biederer, J., Mirsadraee, S., Beer, M., Molinari, F., Hintze, C., Bauman, G., Both, M., Van Beek, E.J., Wild, J. & Puderbach, M. 2012, "MRI of the lung (3/3)—current applications and future perspectives", *Insights into imaging,* , pp. 1-14.

Blé, F., Cannet, C., Zurbruegg, S., Karmouty-Quintana, H., Bergmann, R., Frossard, N., Trifilieff, A. & Beckmann, N. 2008, "Allergen-induced Lung Inflammation in Actively Sensitized Mice Assessed with MR Imaging 1", *Radiology,* vol. 248, no. 3, pp. 834-843.

Boone, J.M., Velazquez, O. & Cherry, S.R. 2004, "Small-animal X-ray dose from micro-CT", *Molecular imaging,* vol. 3, no. 3, pp. 149-158.

Bottomley, P.A., Foster, T.H., Argersinger, R.E. & Pfeifer, L.M. 1984, "A review of normal tissue hydrogen NMR relaxation times and relaxation mechanisms from 1-100 MHz: dependence on tissue type, NMR frequency, temperature, species, excision, and age.", *Medical physics,* vol. 11, no. 4, pp. 425.

Buzan, M.T., Eichinger, M., Kreuter, M., Kauczor, H., Herth, F.J., Warth, A., Pop, C.M., Heussel, C.P. & Dinkel, J. 2015, "T2 mapping of CT remodelling patterns in interstitial lung disease", *European radiology,* , pp. 1-8.

Chen, Q., Jakob, P.M., Griswold, M.A., Levin, D.L., Hatabu, H. & Edelman, R.R. 1998, "Oxygen enhanced MR ventilation imaging of the lung", *Magnetic Resonance Materials in Physics, Biology and Medicine,* vol. 7, no. 3, pp. 153-161.

Costa, G.M., Faria, A.C.D., Mango, D., Tavares, A.M.G., Lopes, A.J., Jansen, J.M. & Melo, P.L. 2009, "Bronchodilation in COPD: beyond FEV1-the effect of albuterol on resistive and reactive properties of the respiratory system", *Jornal Brasileiro de Pneumologia,* vol. 35, no. 4, pp. 325-333.

Coxson, H.O., Dirksen, A., Edwards, L.D., Yates, J.C., Agusti, A., Bakke, P., Calverley, P.M., Celli, B., Crim, C. & Duvoix, A. 2013, "The presence and progression of emphysema in COPD as determined by CT scanning

and biomarker expression: a prospective analysis from the ECLIPSE study", *The lancet Respiratory medicine,* vol. 1, no. 2, pp. 129-136.
Dasenbrook, E.C., Lu, L., Donnola, S., Weaver, D.E., Gulani, V., Jakob, P.M., Konstan, M.W. & Flask, C.A. 2013, "Normalized T1 Magnetic Resonance Imaging for Assessment of Regional Lung Function in Adult Cystic Fibrosis Patients-A Cross-Sectional Study", *PloS one,* vol. 8, no. 9, pp. e73286.
Deoni, S.C., Peters, T.M. & Rutt, B.K. 2004, "Determination of optimal angles for variable nutation proton magnetic spin-lattice, T1, and spin-spin, T2, relaxation times measurement", *Magnetic Resonance in Medicine,* vol. 51, no. 1, pp. 194-199.
Deoni, S.C., Rutt, B.K. & Peters, T.M. 2003, "Rapid combined T1 and T2 mapping using gradient recalled acquisition in the steady state", *Magnetic Resonance in Medicine,* vol. 49, no. 3, pp. 515-526.
Devereux, G. 2006, "ABC of chronic obstructive pulmonary disease: definition, epidemiology, and risk factors", *BMJ: British Medical Journal,* vol. 332, no. 7550, pp. 1142.
Edelman, R.R., Hatabu, H., Tadamura, E., Li, W. & Prasad, P.V. 1996, "Noninvasive assessment of regional ventilation in the human lung using oxygen–enhanced magnetic resonance imaging", *Nature medicine,* vol. 2, no. 11, pp. 1236-1239.
Edirisinghe, I., Yang, S.R., Yao, H., Rajendrasozhan, S., Caito, S., Adenuga, D., Wong, C., Rahman, A., Phipps, R.P., Jin, Z.G. & Rahman, I. 2008, "VEGFR-2 inhibition augments cigarette smoke-induced oxidative stress and inflammatory responses leading to endothelial dysfunction", *FASEB journal : official publication of the Federation of American Societies for Experimental Biology,* vol. 22, no. 7, pp. 2297-2310.
Fain, S.B., Panth, S.R., Evans, M.D., Wentland, A.L., Holmes, J.H., Korosec, F.R., O'Brien, M.J., Fountaine, H. & Grist, T.M. 2006, "Early Emphysematous Changes in Asymptomatic Smokers: Detection with 3He MR Imaging 1", *Radiology,* vol. 239, no. 3, pp. 875-883.
Faller, A., Schünke, M., Schünke, G. & Taub, E. 2004, *The human body: an introduction to structure and function,* Thieme.
Gold, G.E., Han, E., Stainsby, J., Wright, G., Brittain, J. & Beaulieu, C. 2004, "Musculoskeletal MRI at 3.0 T: relaxation times and image contrast", *American Journal of Roentgenology,* vol. 183, no. 2, pp. 343-351.
Gowland, P.A. 2003, "Ti: the Longitudinal Relaxation Time", *Quantitative MRI of the brain: Measuring changes caused by disease,* , pp. 111.
Haddock, B., Larsson, H.B., Hansen, A.E. & Rostrup, E. 2013, "Measurement of brain oxygenation changes using dynamic T 1-weighted imaging", *NeuroImage,* vol. 78, pp. 7-15.

Hanrahan, J.P., Sherman, C.B., Bresnitz, E.A., Emmons, K.M. & Mannino, D.M. 1996, "Cigarette smoking and health. American Thoracic Society.", *American Journal of Respiratory and Critical Care Medicine,* vol. 153, no. 2, pp. 861-865.

Hatabu, H., Tadamura, E., Chen, Q., Stock, K.W., Li, W., Prasad, P.V. & Edelman, R.R. 2001, "Pulmonary ventilation: dynamic MRI with inhalation of molecular oxygen", *European Journal of Radiology,* vol. 37, no. 3, pp. 172-178.

Hofman, M.S., Beauregard, J.M., Barber, T.W., Neels, O.C., Eu, P. & Hicks, R.J. 2011, "68Ga PET/CT ventilation-perfusion imaging for pulmonary embolism: a pilot study with comparison to conventional scintigraphy", *Journal of nuclear medicine : official publication, Society of Nuclear Medicine,* vol. 52, no. 10, pp. 1513-1519.

Homer, J. & Beevers, M.S. 1985, "Driven-equilibrium single-pulse observation of T1 relaxation. A reevaluation of a rapid “new” method for determining NMR spin-lattice relaxation times", *Journal of Magnetic Resonance (1969),* vol. 63, no. 2, pp. 287-297.

Hopkins, S.R., Henderson, A.C., Levin, D.L., Yamada, K., Arai, T., Buxton, R.B. & Prisk, G.K. 2007, "Vertical gradients in regional lung density and perfusion in the supine human lung: the Slinky effect", *Journal of applied physiology (Bethesda, Md.: 1985),* vol. 103, no. 1, pp. 240-248.

Hubbard, P.L., Parker, G.J., Singh, D., Bondesson, E., Olsson, L.E., Wigström, L., Young, S.S. & Naish, J.H. 2011, *Heterogeneity of the ventilation–perfusion ratio in lung disease using OE-MRI*. Proc. Intl. Soc. Mag. Reson. Med. 19.

Irvin, C.G. & Bates, J. 2003, "Measuring the lung function in the mouse: the challenge of size", *Respir Res,* vol. 4, no. 4, pp. 1-9.

Jakob, P.M., Hillenbrand, C.M., Wang, T., Schultz, G., Hahn, D. & Haase, A. 2001, "Rapid quantitative lung (1)H T(1) mapping", *Journal of magnetic resonance imaging : JMRI,* vol. 14, no. 6, pp. 795-799.

Jiao, X. & Bryant, R.G. 1996, "Noninvasive measurement of protein concentration", *Magnetic resonance in medicine,* vol. 35, no. 2, pp. 159-161.

Jögi, J., Ekberg, M., Jonson, B., Bozovic, G. & Bajc, M. 2011, "Ventilation/perfusion SPECT in chronic obstructive pulmonary disease: an evaluation by reference to symptoms, spirometric lung function and emphysema, as assessed with HRCT", *European journal of nuclear medicine and molecular imaging,* vol. 38, no. 7, pp. 1344-1352.

Johnson, K.M., Fain, S.B., Schiebler, M.L. & Nagle, S. 2013, "Optimized 3D ultrashort echo time pulmonary MRI", *Magnetic Resonance in Medicine,* vol. 70, no. 5, pp. 1241-1250.

Jones, P. & Agusti, A. 2006, "Outcomes and markers in the assessment of chronic obstructive pulmonary disease", *European Respiratory Journal,* vol. 27, no. 4, pp. 822-832.

Karimi, R., Tornling, G., Forsslund, H., Mikko, M., Wheelock, A., Nyren, S. & Skold, C.M. 2014, "Lung density on high resolution computer tomography (HRCT) reflects degree of inflammation in smokers", *Respiratory research,* vol. 15, pp. 23-9921-15-23.

Katzenstein, A.A. & Myers, J.L. 1998, "Idiopathic pulmonary fibrosis: clinical relevance of pathologic classification", *American journal of respiratory and critical care medicine,* vol. 157, no. 4, pp. 1301-1315.

Kauczor, H. & Altes, T.A. 2009, *MRI of the Lung,* Springer Science & Business Media.

Kilburn, K.H. 1984, "Particles causing lung disease.", *Environmental health perspectives,* vol. 55, pp. 97.

Kingsley, P.B. & Gordon Monahan, W. 2001, "Effect of increased repetition time TR on precision of inversion-recovery T1 measurements", *Magnetic resonance imaging,* vol. 19, no. 2, pp. 279-282.

Kruger, S.J., Nagle, S.K., Couch, M.J., Ohno, Y., Albert, M. & Fain, S.B. 2015, "Functional imaging of the lungs with gas agents", *Journal of Magnetic Resonance Imaging,* .

Kveder, M., Zupancic, I., Lahajnar, G., Blinc, R., Suput, D., Ailion, D.C., Ganesan, K. & Goodrich, C. 1988, "Water proton NMR relaxation mechanisms in lung tissue", *Magnetic resonance in medicine : official journal of the Society of Magnetic Resonance in Medicine / Society of Magnetic Resonance in Medicine,* vol. 7, no. 4, pp. 432-441.

Lankton, S. & Tannenbaum, A. 2008, "Localizing region-based active contours", *Image Processing, IEEE Transactions on,* vol. 17, no. 11, pp. 2029-2039.

Laurent, W., Bonny, J. & Renou, J. 2000, "Imaging of water and fat fractions in high-field MRI with multiple slice chemical shift-selective inversion recovery", *Journal of Magnetic Resonance Imaging,* vol. 12, no. 3, pp. 488-496.

Lederlin, M. & Crémillieux, Y. 2014, "Three-dimensional assessment of lung tissue density using a clinical ultrashort echo time at 3 tesla: A feasibility study in healthy subjects", *Journal of Magnetic Resonance Imaging,* vol. 40, no. 4, pp. 839-847.

Lum, H. & Mitzner, W. 1987, "A species comparison of alveolar size and surface forces", *Journal of applied physiology (Bethesda, Md.: 1985),* vol. 62, no. 5, pp. 1865-1871.

Lynch, D.A. 2008, "Imaging of small airways disease and chronic obstructive pulmonary disease", *Clinics in chest medicine,* vol. 29, no. 1, pp. 165-179.

Mai, V.M., Chen, Q., Li, W., Hatabu, H. & Edelman, R.R. 2000, "Effect of respiratory phases on MR lung signal intensity and lung conspicuity using segmented multiple inversion recovery turbo spin echo (MIR-TSE)", *Magnetic resonance in medicine,* vol. 43, no. 5, pp. 760-763.

Mannino, D.M., Watt, G., Hole, D., Gillis, C., Hart, C., McConnachie, A., Davey Smith, G., Upton, M., Hawthorne, V., Sin, D.D., Man, S.F.P., Van Eeden, S., Mapel, D.W. & Vestbo, J. 2006, "The natural history of chronic obstructive pulmonary disease", *European Respiratory Journal,* vol. 27, no. 3, pp. 627-643.

Markstaller, K., Eberle, B., Schreiber, W.G., Weiler, N., Thelen, M. & Kauczor, H. 2000, "Flip angle considerations in 3Helium-MRI", *NMR in biomedicine,* vol. 13, no. 4, pp. 190-193.

Marsh, S., Aldington, S., Shirtcliffe, P., Weatherall, M. & Beasley, R. 2006, "Smoking and COPD: what really are the risks?", *European Respiratory Journal,* vol. 28, no. 4, pp. 883-884.

Mirsadraee, S. & van Beek, E.J. 2015, "Functional Imaging: Computed Tomography and MRI", *Clinics in chest medicine,* vol. 36, no. 2, pp. 349-363.

Morgan, A.R., Parker, G.J., Roberts, C., Buonaccorsi, G.A., Maguire, N.C., Cristinacce, P.L.H., Singh, D., Vestbo, J., Bjermer, L. & Jögi, J. 2014, "Feasibility assessment of using oxygen-enhanced magnetic resonance imaging for evaluating the effect of pharmacological treatment in COPD", *European Journal of Radiology,* vol. 83, no. 11, pp. 2093-2101.

Nakagawa, T., Sakuma, H., Murashima, S., Ishida, N., Matsumura, K. & Takeda, K. 2001, "Pulmonary ventilation-perfusion MR imaging in clinical patients", *Journal of Magnetic Resonance Imaging,* vol. 14, no. 4, pp. 419-424.

Nakano, Y., Muro, S., Sakai, H., Hirai, T., Chin, K., Tsukino, M., Nishimura, K., Itoh, H., Pare, P.D. & Hogg, J.C. 2000, "Computed tomographic measurements of airway dimensions and emphysema in smokers: correlation with lung function", *American journal of respiratory and critical care medicine,* vol. 162, no. 3, pp. 1102-1108.

Nordin, G., Mårtensson, A., Swolin, B., Sandberg, S., Christensen, N., Thorsteinsson, V., Franzson, L., Kairisto, V. & Savolainen, E. 2004, "A multicentre study of reference intervals for haemoglobin, basic blood cell counts and erythrocyte indices in the adult population of the Nordic countries", *Scandinavian journal of clinical & laboratory investigation,* vol. 64, no. 4, pp. 385-398.

Ohno, Y. & Hatabu, H. 2007, "Basics concepts and clinical applications of oxygen-enhanced MR imaging", *European Journal of Radiology,* vol. 64, no. 3, pp. 320-328.

Ohno, Y., Koyama, H., Yoshikawa, T., Seki, S., Takenaka, D., Yui, M., Lu, A., Miyazaki, M. & Sugimura, K. 2015, "Pulmonary high-resolution ultrashort TE MR imaging: Comparison with thin-section standard-and low-dose computed tomography for the assessment of pulmonary parenchyma diseases", *Journal of Magnetic Resonance Imaging, .*

Ohno, Y., Iwasawa, T., Seo, J.B., Koyama, H., Takahashi, H., Oh, Y.M., Nishimura, Y. & Sugimura, K. 2008, "Oxygen-enhanced magnetic resonance imaging versus computed tomography: multicenter study for clinical stage classification of smoking-related chronic obstructive pulmonary disease", *American journal of respiratory and critical care medicine,* vol. 177, no. 10, pp. 1095-1102.

Olsson, L.E., Lindahl, M., Önnervik, P., Johansson, L.B., Palmér, M., Reimer, M.K., Hultin, L. & Hockings, P.D. 2007a, "Measurement of MR signal and T2* in lung to characterize a tight skin mouse model of emphysema using single-point imaging", *Journal of Magnetic Resonance Imaging,* vol. 25, no. 3, pp. 488-494.

Olsson, L.E., Lindahl, M., Önnervik, P., Johansson, L.B., Palmér, M., Reimer, M.K., Hultin, L. & Hockings, P.D. 2007b, "Measurement of MR signal and T2* in lung to characterize a tight skin mouse model of emphysema using single-point imaging", *Journal of Magnetic Resonance Imaging,* vol. 25, no. 3, pp. 488-494.

Pauwels, R.A. & Rabe, K.F. 2004, "Burden and clinical features of chronic obstructive pulmonary disease (COPD)", *The Lancet,* vol. 364, no. 9434, pp. 613-620.

Renne, J., Lauermann, P., Hinrichs, J., Schönfeld, C., Sorrentino, S., Gutberlet, M., Jakob, P., Wacker, F. & Vogel-Claussen, J. 2015, "Clinical use of oxygen-enhanced T1 mapping MRI of the lung: Reproducibility and impact of closed versus loose fit oxygen delivery system", *Journal of Magnetic Resonance Imaging,* vol. 41, no. 1, pp. 60-66.

Roy, K., Smith, J., Kolsum, U., Borrill, Z., Vestbo, J. & Singh, D. 2009, "COPD phenotype description using principal components analysis", *Respir Res,* vol. 10, no. 1, pp. 41.

Schabel, M.C. & Morrell, G.R. 2009, "Uncertainty in T1 mapping using the variable flip angle method with two flip angles", *Physics in Medicine and Biology,* vol. 54, no. 1, pp. N1.

Schaefer-Prokop, C., Neitzel, U., Venema, H.W., Uffmann, M. & Prokop, M. 2008, "Digital chest radiography: an update on modern technology, dose containment and control of image quality", *European radiology,* vol. 18, no. 9, pp. 1818-1830.

Scholz, T.D., Fleagle, S.R., Burns, T.L. & Skorton, D.J. 1989, "Tissue determinants of nuclear magnetic resonance relaxation times. Effect of

water and collagen content in muscle and tendon", *Investigative radiology,* vol. 24, no. 11, pp. 893-898.
Severinghaus, J.W. 1979a, "Simple, accurate equations for human blood O2 dissociation computations", *Journal of applied physiology: respiratory, environmental and exercise physiology,* vol. 46, no. 3, pp. 599-602.
Severinghaus, J.W. 1979b, "Simple, accurate equations for human blood O2 dissociation computations", *Journal of applied physiology: respiratory, environmental and exercise physiology,* vol. 46, no. 3, pp. 599-602.
Shapiro, S.D. 2000, "Animal models for COPD", *CHEST Journal,* vol. 117, no. 5_suppl_1, pp. 223S-227S.
Silvennoinen, M.J., Kettunen, M.I. & Kauppinen, R.A. 2003a, "Effects of hematocrit and oxygen saturation level on blood spin-lattice relaxation", *Magnetic resonance in medicine,* vol. 49, no. 3, pp. 568-571.
Silvennoinen, M.J., Kettunen, M.I. & Kauppinen, R.A. 2003b, "Effects of hematocrit and oxygen saturation level on blood spin-lattice relaxation", *Magnetic resonance in medicine,* vol. 49, no. 3, pp. 568-571.
Skjørten, I., Hilde, J.M., Melsom, M.N., Hansteen, V., Steine, K. & Humerfelt, S. 2013, "Pulmonary artery pressure and PaO 2 in chronic obstructive pulmonary disease", *Respiratory medicine,* vol. 107, no. 8, pp. 1271-1279.
Stadler, A., Jakob, P.M., Griswold, M., Barth, M. & Bankier, A.A. 2005, "T1 mapping of the entire lung parenchyma: influence of the respiratory phase in healthy individuals", *Journal of magnetic resonance imaging,* vol. 21, no. 6, pp. 759-764.
Stadler, A., Jakob, P.M., Griswold, M., Stiebellehner, L., Barth, M. & Bankier, A.A. 2007, "T1 mapping of the entire lung parenchyma: Influence of respiratory phase and correlation to lung function test results in patients with diffuse lung disease", *Magnetic Resonance in Medicine,* vol. 59, no. 1, pp. 96-101.
Stevenson, C.S. & Birrell, M.A. 2011, "Moving towards a new generation of animal models for asthma and COPD with improved clinical relevance", *Pharmacology & therapeutics,* vol. 130, no. 2, pp. 93-105.
Stockley, R.A., Mannino, D. & Barnes, P.J. 2009, "Burden and pathogenesis of chronic obstructive pulmonary disease", *Proceedings of the American Thoracic Society,* vol. 6, no. 6, pp. 524-526.
Swanney, M.P., Ruppel, G., Enright, P.L., Pedersen, O.F., Crapo, R.O., Miller, M.R., Jensen, R.L., Falaschetti, E., Schouten, J.P. & Hankinson, J.L. 2008, "Using the lower limit of normal for the FEV1/FVC ratio reduces the misclassification of airway obstruction", *Thorax,* vol. 63, no. 12, pp. 1046-1051.

Takahashi, M., Fukuoka, J., Nitta, N., Takazakura, R., Nagatani, Y., Murakami, Y., Otani, H. & Murata, K. 2008, "Imaging of pulmonary emphysema: a pictorial review", *International journal of chronic obstructive pulmonary disease,* vol. 3, no. 2, pp. 193-204.

Takahashi, M., Togao, O., Obara, M., van Cauteren, M., Ohno, Y., Doi, S., Kuro-O, M., Malloy, C., Hsia, C.C. & Dimitrov, I. 2010, "Ultra-short echo time (UTE) MR imaging of the lung: Comparison between normal and emphysematous lungs in mutant mice", *Journal of Magnetic Resonance Imaging,* vol. 32, no. 2, pp. 326-333.

Theilmann, R.J., Arai, T.J., Samiee, A., Dubowitz, D.J., Hopkins, S.R., Buxton, R.B. & Prisk, G.K. 2009, "Quantitative MRI measurement of lung density must account for the change in T 2* with lung inflation", *Journal of Magnetic Resonance Imaging,* vol. 30, no. 3, pp. 527-534.

Thurlbeck, W.M. & Muller, N.L. 1994, "Emphysema: definition, imaging, and quantification", *AJR.American journal of roentgenology,* vol. 163, no. 5, pp. 1017-1025.

Togao, O., Ohno, Y., Dimitrov, I., Hsia, C.C. & Takahashi, M. 2011, "Ventilation/perfusion imaging of the lung using ultra-short echo time (UTE) MRI in an animal model of pulmonary embolism", *Journal of magnetic resonance imaging : JMRI,* .

Triphan, S.M., Breuer, F.A., Gensler, D., Kauczor, H. & Jakob, P.M. 2014, "Oxygen enhanced lung MRI by simultaneous measurement of T1 and T2* during free breathing using ultrashort TE", *Journal of Magnetic Resonance Imaging,* .

Triphan, S.M., Jobst, B.J., Breuer, F.A., Wielpütz, M.O., Kauczor, H., Biederer, J. & Jakob, P.M. 2015, "Echo time dependence of observed T1 in the human lung", *Journal of Magnetic Resonance Imaging,* .

van der Have, F., Vastenhouw, B., Ramakers, R.M., Branderhorst, W., Krah, J.O., Ji, C., Staelens, S.G. & Beekman, F.J. 2009, "U-SPECT-II: An Ultra-High-Resolution Device for Molecular Small-Animal Imaging", *Journal of nuclear medicine : official publication, Society of Nuclear Medicine,* vol. 50, no. 4, pp. 599-605.

van Echteld, C.J. & Beckmann, N. 2011, "A view on imaging in drug research and development for respiratory diseases", *The Journal of pharmacology and experimental therapeutics,* vol. 337, no. 2, pp. 335-349.

Vinitski, S., Pearson, M.G., Karlik, S.J., Morgan, W.K., Carey, L.S., Perkins, G., Goto, T. & Befus, D. 1986, "Differentiation of parenchymal lung disorders with in vitro proton nuclear magnetic resonance", *Magnetic resonance in medicine : official journal of the Society of Magnetic Resonance in Medicine / Society of Magnetic Resonance in Medicine,* vol. 3, no. 1, pp. 120-125.

Walker, S.C., Asadi, A.K., Hopkins, S.R., Buxton, R.B. & Prisk, G. 2015, "A statistical clustering approach to discriminating perfusion from conduit vessel signal contributions in a pulmonary ASL MR image", *NMR in biomedicine,* .

Wang, H.Z., Riederer, S.J. & Lee, J.N. 1987, "Optimizing the precision in T1 relaxation estimation using limited flip angles", *Magnetic Resonance in Medicine,* vol. 5, no. 5, pp. 399-416.

Waterton, J. 2013, "Translational magnetic resonance imaging and spectroscopy: opportunities and challenges" in *New Applications of NMR in Drug Discovery and Development*, eds. L. Garrido & N. Beckmann, Royal Society of Chemistry, , pp. 333-360.

Wild, J., Marshall, H., Bock, M., Schad, L., Jakob, P., Puderbach, M., Molinari, F., Van Beek, E. & Biederer, J. 2012, "MRI of the lung (1/3): methods", *Insights into imaging,* vol. 3, no. 4, pp. 345-353.

Wille, M.M.W., Thomsen, L.H., Dirksen, A., Petersen, J., Pedersen, J.H. & Shaker, S.B. 2014, "Emphysema progression is visually detectable in low-dose CT in continuous but not in former smokers", *European radiology,* vol. 24, no. 11, pp. 2692-2699.

Yamamoto, S., Watabe, H., Kanai, Y., Imaizumi, M., Watabe, T., Shimosegawa, E. & Hatazawa, J. 2011, "Development of a high-resolution Si-PM-based gamma camera system", *Physics in Medicine and Biology,* vol. 56, no. 23, pp. 7555.

Yu, J., Xue, Y. & Song, H.K. 2011, "Comparison of lung T2* during free-breathing at 1.5 T and 3.0 T with ultrashort echo time imaging", *Magnetic Resonance in Medicine,* vol. 66, no. 1, pp. 248-254.

Zhang, Y., Hetherington, H.P., Stokely, E.M., Mason, G.F. & Twieg, D.B. 1998, "A novel k-space trajectory measurement technique", *Magnetic Resonance in Medicine,* vol. 39, no. 6, pp. 999-1004.